LOCAL DELIVERY OF FTY720 FROM TISSUE DERIVED MATRICES FOR BONE GRAFT INTEGRATION

A Thesis
Presented to
The Academic Faculty

by

Tiffany Wang

In Partial Fulfillment
of the Requirements for the Degree
Master of Science in the
School of Biomedical Engineering

Georgia Institute of Technology
December 2013

LOCAL DELIVERY OF FTY720 FROM TISSUE DERIVED MATRICE FOR BONE GRAFT INTEGRATION

Approved by:

Dr. Edward Botchwey, Advisor
School of Biomedical Engineering
Georgia Institute of Technology

Dr. Thomas Barker
School of Biomedical Engineering
Georgia Institute of Technology

Dr. Roy Ogle
School of Medical Diagnostics and Translational Science
Old Dominion University

Date Approved: November 7, 2013

ACKNOWLEDGEMENTS

I sincerely thank my advisor Dr. Ed Botchwey for all the support and guidance he has given me, as well for giving me the opportunity to join him at Georgia Tech. I want to thank my committee members Dr. Roy Ogle and Dr. Thomas Barker for their valuable feedback on my work. I want to thank the Botchwey lab members past and present for their friendship and support. And finally, I want to express my love and gratitude to my family and friends.

TABLE OF CONTENTS

LIST OF FIGURES

SUMMARY

Despite advances in bone grafting technology for musculoskeletal injury, re-injury or incomplete healing persists. Efforts to modify bone allografts using proteins and growth factors show improvement in wound healing outcomes. This thesis uses FTY720, an agonist of S1P receptors 1 and 3, to improve bone graft integration through bone regeneration and vascularization. Four methods of delivering FTY720 into a bone defect are described:

1) FTY720 loaded onto a PLAGA-coated bone allograft and implanted in a critical size rat cranial defect.
2) FTY720 loaded onto a PLAGA graft and implanted in a rat tibial defect.
3) FTY720 loaded into a Matrigel plug and injected in a mouse tibial defect.
4) FTY720 directly adsorbed to human bone xenografts and implanted in a critical size rat cranial defect.

In each of these models, FTY720 release was characterized, and bone regeneration and vascularization was monitored within the defect. Additionally, local tissue composition was evaluated.

The results presented in this thesis indicate that FTY720 released locally into the bone defect improved new bone formation and vascularization, promoting improved graft integration.

CHAPTER 1

INTRODUCTION

1.1 Clinical Need for Bone Grafting Technologies

Each year, nearly $510 billion is spent in the United States to treat musculoskeletal conditions [1], amounting to nearly 2.4 million procedures in 2011 [2]. Of that, $2.5 billion is spent on bone grafting procedures after incidents such as wartime trauma, accidents, bone resections, spinal fusions, and periodontal procedures [3]. As with the implantation of any material into the body, there are a variety of factors to consider. These include the biocompatibility and immunogenicity of the implant material, its ability to integrate with and be remodeled by the host tissue, as well as its biomechanical compatibility with the structure and function of the injured region [4]. In general, cortical bone is more load-bearing, and takes more time to revascularize than cancellous bone, which tends to be more porous [4]. Additionally, cancellous bone experiences creeping substitution, whereby osteoblasts, osteoclasts and endothelial cells can move towards the central mass of the graft and remodel as they go, whereas in cortical bone, osteoclasts first have to digest existing mineralized matrix to make way for cellular infiltration [4]. Therefore, it is important to consider whether the injured bone is of the cortical or cancellous variety, which would influence which graft material would be most suitably applied to restore the structure and function of the injury.

Grafts can come in the form of human bone (i.e. autografts and allografts), animal bone (xenografts), and can also be composed of synthetic and natural polymers [4,5,6]. Commonly used polymers include collagen [7,8,9], poly(lactic co-glycolic acid)(PLAGA) [9], poly(ethylene glycol)(PEG) [9,10,11]. Strategies have been evaluated

in animal models of bone defects that combine both natural and synthetic materials to promote bone regeneration and graft integration.

1.2 Autografts for Bone Repair

Autografts are harvested from one site on the patient's body and transplanted to another site to aid in wound healing. This procedure remains the current gold standard of treatment for bone tissue grafting because it maintains the osteogenic cell types necessary for new bone formation, as well as the osteoconductive mineral matrix that guides new bone deposition. Autografts are also not challenged with the risk of immune rejection or disease transmission, two complications commonly associated with transplants from other donors or cadavers. A common source of autograft bone is the iliac crest, as it can provide a relatively large volume of bone without damaging the structural integrity and function of the source area [12]. However, the creation of a second would site on the patient can cause complications such as donor site morbidity and infection if the area is not cared for properly [13,14,15]. Additionally, the limited supply of autograft bone leads to complication in matching the bone graft type to the wound area. In the table compiled by Brydone *et.al.*, it is documented that different types of bone have differing characteristics, specifically for structural strength [16]. A more structurally porous cancellous bone graft may be unable to recapitulate the load bearing properties experienced by cortical long bone, and would therefore be less ideal to use as a graft in a cortical long bone injury. The limited ability to match bone graft type with the bone type in the wound area makes allografts an attractive option.

1.3 Allografts for Bone Repair

Allografts are harvested from donors and cadavers, and are used extensively to repair bone wounds. This bone source eliminates the creation of a second wound site on the patient; however, in the case of a living donor, this procedure creates a second patient. A

significant advantage of using allografts in wound repair is a larger and more varied supply – bone material can be harvested from cadavers and donors to meet the specific size and structural requirements of the bone injury.

A variety of techniques have been developed to reduce the potential immunogenicity of allograft material. Deep-freezing and freeze-drying have both been used to reduce the immunogenicity of the harvested tissue [17] by stripping away cellularized material from the mineral matrix. However, there are still reported cases that these decellularized grafts still cause chronic inflammation and a non-specific immune response [17]. Additionally, there is some evidence that the freeze-drying process diminishes the mechanical integrity of the scaffold structure [18]. There has also been some success using these freeze-drying techniques to allow for long term storage of harvested allograft material [19]. The ability to harvest and bank human allograft material is attractive, especially in environments that experience high incidences of bone injury, such as a battlefield environment. There do still exist complications in the allograft banking effort, as there have been reports of biological contamination on the grafts after long term storage, as well as residual chemical contamination on the grafts that originate from the sterilization process [17,19]. In order for long term banking of bone allografts to be possible, there are still some technologies that have to be further refined.

Even if using allografts addresses issues such as matching graft size and structure to the wound area, poor graft vascularization and remodeling can still lead to eventual graft failure due to infection and poor integration [20]. It has been observed clinically that massive allografts experience a 30-60% failure rate [20], and allografts in general lose 50% of their mechanical integrity over 10 years [21]. It is therefore vital to find ways to improve graft integration and vascularization to prolong the functioning lifetime of the graft. The decellularization processes preserves the osteoconductive nature of the

mineralized scaffold, but it strips away the osteogenic potential of the resident osteoblasts and osteoclasts, which have to be replaced by some other means.

1.4 Sphingosine 1-phosphate is a Small Bioactive Signaling Lipid in Bone Regeneration and Vascularization

Sphingosine 1-phosphate (S1P) is a pleiotropic, autocrine- and paracrine-signaling sphingolipid that is released into the blood upon platelet activation [22]. It acts extracellularly by binding to a family of five high affinity G-protein coupled receptors ($S1P_1$-$S1P_5$), and it acts intracellularly as a signaling metabolite to govern a wide range of biological processes that play roles in wound healing.

1.4.1 The role of S1P in bone regeneration

In the case of decellularized allografts, it is necessary to provide local cues to recruit osteoprogenitor cells to the wound area in order to begin remodeling the graft. Ishii *et.al.*

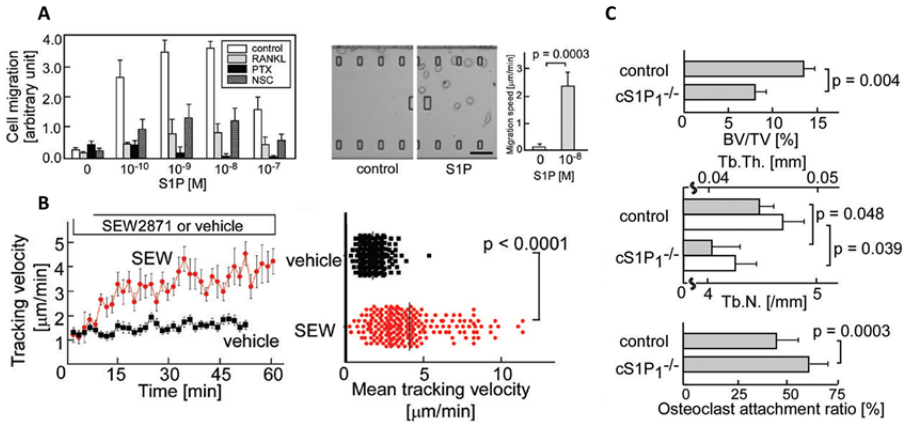

Fig 1.1: S1P mediated migration of RAW264.7 macrophages. A) Cell migration is increased towards S1P in the absence of inhibitors. B) Cell migration velocity increases with application of SEW2871, a potent $S1P_1$ agonist. C) Total bone volume and bone density decrease in S1P1deficient mice, while osteoclast attachment increases [23].

demonstrated that signaling on the S1P-$S1P_1$ axis promoted the migration of osteoprogenitor cells towards higher concentrations of S1P *in vitro* (Fig 1.1A) [23]. Additionally, Ishii *et.al.* tracked cell mobility using two-photon intravital microscopy in

CX_3CR1-EGFP mice, specifically looking in the bone marrow stromal cell compartment or at the bone surface. They observed that pharmacological stimulation of this signaling axis using SEW2871, a potent $S1P_1$ agonist, further increases the motility of osteoprogenitor cells out of the bone marrow, and along the S1P gradient (Fig 1.1B) [23]. Finally, they observed that in $S1P_1$ deficient mice, measurement of steady state bone volume, trabecular thickness and trabecular density were decreased, while osteoclast attachment was increased (Fig 1.1C) [23]. In the absence of $S1P_1$, osteoprogenitor cells are not drawn back into the circulation along the present S1P gradient, and therefore remain in the bone tissue and mature into osteoclasts, which is observed in the increased osteoclast attachment and osteoclast activity in the $S1P_1$ mice.

S1P was shown to increase the chemotaxis of osteoblasts and T-cells towards

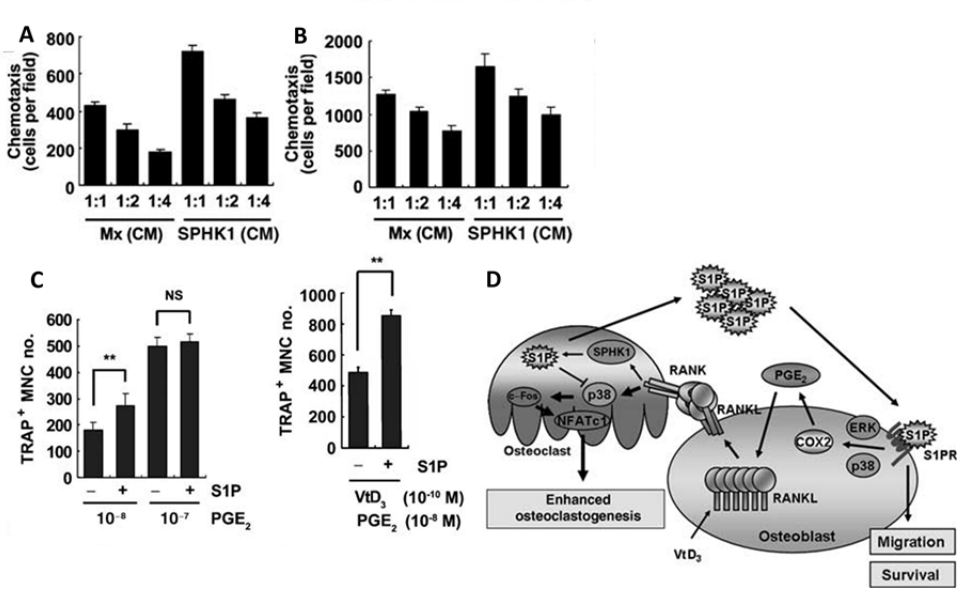

Fig 1.2: S1P regulates osteoclastogenesis via RANKL expression regulated by a PGE2 and COX2 pathway. A) S1P increases osteoblast migration towards SPK1. B) S1P increases T-cell migration towards SPK1. C) Increased osteoclast generation from bone marrow macrophages stimulated with S1P. D) S1P promotes osteoclastogenesis [24].

SPK1 activity as indicated by migration towards conditioned media from SPK1-overexpressing differentiating bone marrow macrophages (Fig 1.2A,B). The addition of exogenous S1P to co-culture of bone marrow-derived macrophages (BMM) and osteoblasts has been shown to increase osteoclast generation by increasing RANKL

production in osteoblasts through PGE_2 regulation (Fig 1.2C) [24]. Taken together, Ryu et.al. assert that BMMs produce extracellular S1P in response to RANKL, which binds to S1P receptors on osteoblasts, which then upregulates COX2 and PGE_2. PGE_2 further induces RANKL expression, leading to osteoclastogenesis (Fig 1.2D). Increased osteoclastogenesis as promoted by S1P is useful for bone matrix remodeling in bone regeneration.

It has also been shown that mature osteoclasts exhibit increased S1P production via SPK1 compared to pre-osteoclasts (Fig 1.3A,B) [25]. They also elucidated that mineral deposition by human mesenchymal stem cells (hMS) was decreased when Wnt activity was blocked using DKK, or $S1P_1$ activity was blocked using an the antagonist PC23019, after 7 days (Fig1.3C) [25]. Therefore, S1P signaling in concert with Wnt signaling is necessary for mineral deposition, which is an important step in bone regeneration.

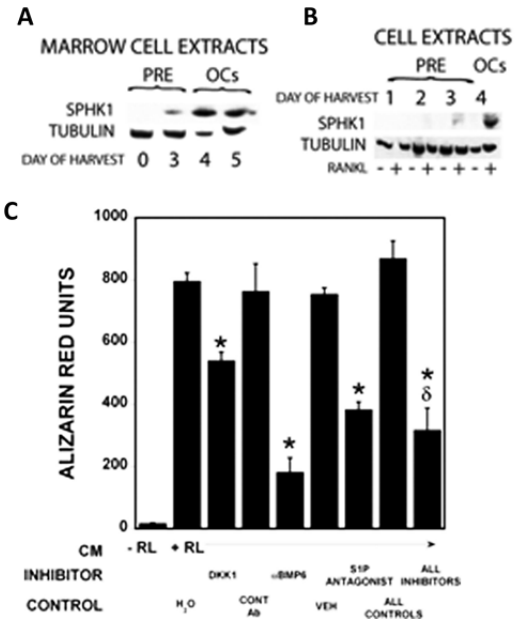

Fig 1.3: S1P and Wnt signaling in mineral deposition. A) Bone marrow cell-derived mature osteoclasts have increased levels of SPK1. B) RAW macrophage derived mature osteoclasts have increased levels of SPK1. C) Blocking Wnt signaling (DKK) and S1P signaling (S1P antagonist) decrease mineral deposition by hMS [25].

Finally, S1P has been shown to have a role in hematopoietic progenitor cell egress from the bone marrow. Golan *et.al.* observed that desensitization of S1P receptors using either FTY720 or DOP, which degrade S1P lyase, caused a decrease in the number of colony forming units from cells harvested from blood of wild type mice (Fig 1.4A) [26]. AMD3100 is clinically used to increase circulating progenitor cells; however AMD3100 treatment on SPK1 KO mice is significantly lower than that of wild type mice (Fig 1.4B) [26]. SDF-1 levels in SPK1

KO mice is also decreased compared to wild type mice after AMD3100 treatment (Fig 1.4C) [26]. They also observed that S1P induced SDF-1 secretion from bone marrow stromal cells is reduced when S1P receptors are desensitized by FTY720 (Fig 1.4D). They assert that therefore the S1P signaling axis regulates AMD3100-induced mobilization of progenitor cells from the bone marrow via SDF-1 levels in the blood.

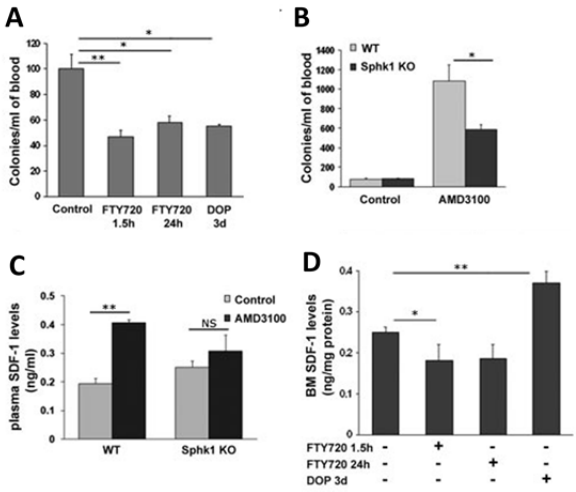

Fig 1.4: S1P signaling regulates AMD3100-induced mobilization of progenitor cells via SDF-1 levels. A) Desensitization of S1P receptors decreases the number of colonies formed by cells harvested from wild type mice. B) AMD3100-treated blood harvested from SPK1 KO mice form fewer colonies in a CFU assay. C) Plasma SDF-1 levels in AMD3100-treated SPK1 KO mice is reduced. D) Bone marrow SDF-1 levels in wild type mice decreased when S1P1 receptors are desensitized with FTY720 [26].

1.4.2 The role of S1P in vascularization

Successful bone regeneration through graft integration also requires vascular infiltration into the graft to support the cells that are depositing and remodeling new bone matrix. As reviewed by Takuwa *et.al.*, S1P acts on endothelial cells to via $S1P_1$ and $S1P_3$ to activate Rac pathways to stimulate angiogenesis (Fig 1.5) [27]. Specifically, it has been found that S1P induces the formation of adherens junctions as shown by the increased α-catenin and VE-cadherin polypeptides in the γ- and β- catenin mmunoprecipitates (Fig 1.6A) [28]. Confocal imaging of VE-cadherin staining (red) confirms the increased formation of adherens junctions when human umbilical vascular

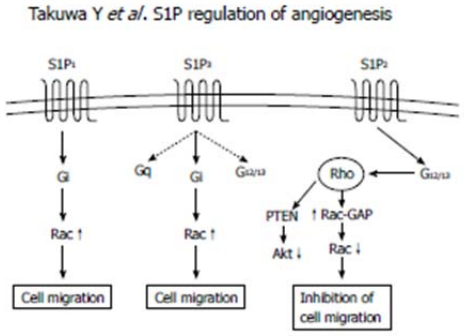

Fig 1.5: S1P activates Rac pathways through S1P receptors to regulate cell migration in angiogenesis [27].

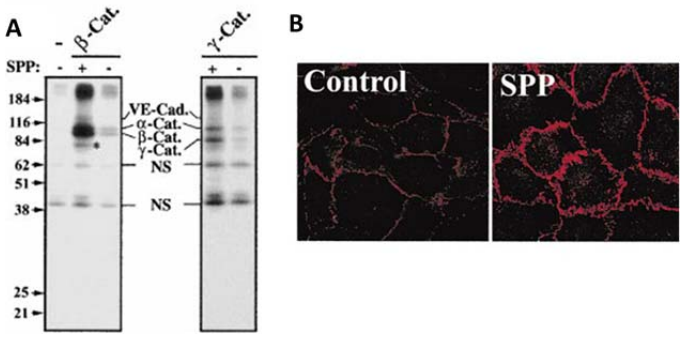

Fig 1.6: S1P promotes formation of adherens junctions. A) Increased α-catenin and VE-cadherin in immunoprecipitate, as well as mutually exclusive presence of β- and γ-catenin in their respective fractions. B) Confocal imaging of VE-cadherin(red) shows increased formation of adherens junctions in HUVECS [28].

endothelial cells are treated with S1P (Fig 1.6B) [28]. Also, S1P activation of $S1P_1$ is known to trigger an Akt-mediated pathway that results in endothelial cell migration. Specifically, $S1P_1$- and $S1P_3$- mediated migration toward S1P was significantly increased in CHO cells transduced with wild type Akt (Fig 1.7A,B) and Rac expression (Fig 1.7C), leading to the conclusion that S1P activation of an Akt pathway leads to increased actin assembly and cell migration (Fig 1.7D) [29]. The increasd presence of S1P, potentially due to increased osteoclasts in the defect area, can further amplify an S1P gradient toward the actively remodeling bone defect, thereby promoting endothelial cell migration in that direction. S1P has also been shown to play a role in recruiting vascular smooth muscle cells to stabilize newly formed vasculature [30], as evidenced by the absence of vascular smooth muscle cells in forming vessels in $S1P_1$ deficient embryos (Fig 1.8).

Olivera *et.al.* has shown that S1P (SPH in the figure) is upregulated in PDGF-mediated proliferation pathways in Swiss 3T3 fibroblasts as indicated by the increased presence of the radiolabeled S1P (Fig 1.9) [31]. Furthermore, Guo et.al. used mesenchymal stem cells transfected with basic fibroblast growth factors seeded onto scaffolds of tricalcium phosphate to improve host-graft integration over 12 weeks (Fig 1.10) [32]. We can conclude that S1P-induced increase of fibroblast proliferation would similarly increase bFGF levels, leading to improved bone graft integration.

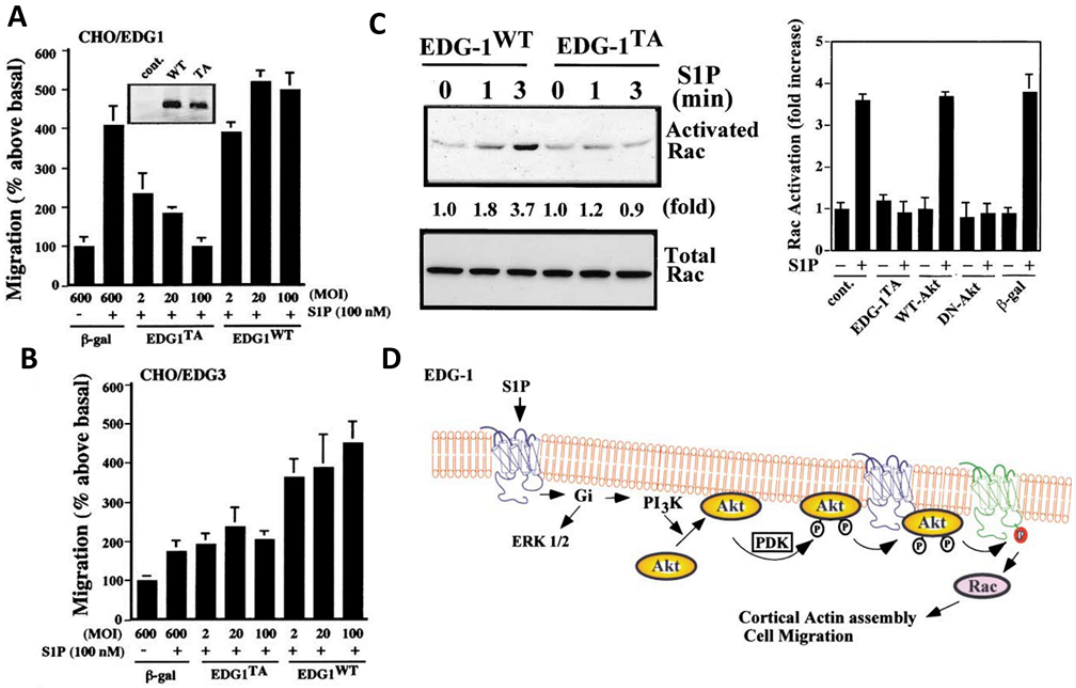

Fig 1.7: S1P-directed endothelial cell migration mediated through an Akt pathway. A) EDG1/S1P1 and B) EDG3/S1P3 mediated migration of CHO cells towards S1P. C) Rac is upregulated in cells with active Akt. D) S1P triggers Akt-mediated cell migration towards S1P [29].

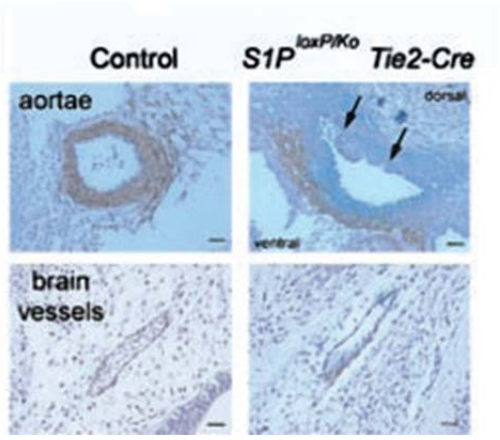

Fig 1.8: $S1P_1$ necessary for recruitment of vascular smooth muscle cells to forming vasculature. Control sections have normal smooth muscle investment of vasculature, but $S1P_1$ mutant embryos do not form normal vasculature [30].

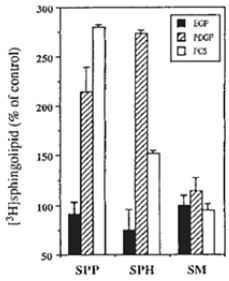

Fig 1.9: S1P is upregulated in PDGF mediated fibroblast proliferation [31].

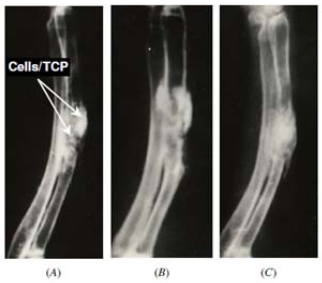

Fig 1.10: MSCs transfected with bFGF seeded onto ceramic scaffolds increases bone-graft integration over 12 weeks in forelimb defect model in rabbits [32].

1.4.3 The role of S1P in lymphocyte trafficking

Successful graft integration also requires minimal immune response to the graft material, preventing graft rejection. Schwab *et.al.* showed that increased concentration of S1P through inhibition of S1P lyase resulted in increased internalization of $S1P_1$ on the surface of lymphocytes, thereby decreasing their egress from lymphoid organs into circulation (Fig 1.11) [33].

Two general classes of macrophages have been characterized as contributing to inflammation and inflammation resolution: the M1 phenotype is pro-inflammatory while the M2 phenotype is more anti-inflammatory and pro-regeneration. Hughes et.al. determined that S1P promotes production of the M2 macrophage through activation of S1P1 receptor [34]. More recently, Awojoodu *et.al.* showed that S1P also acts through S1P3 to preferentially recruit M2 macrophages to sites of arteriogenesis. They show that after transplanting DiI-labeled M2 macrophages into mice, more of those M2

macrophages were recruited into tissue from the blood when animals are treated with an S1P receptor-targeted drug (Fig 1.12) [35].

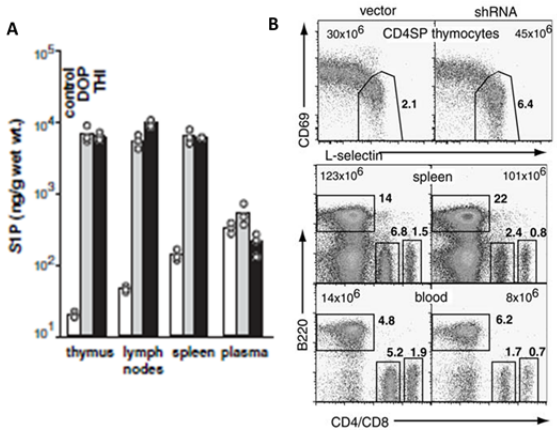

Fig 1.11: Increased S1P concentration leads to increased lymphocyte sequestration. Inhibition of S1P lyase increases S1P concentration, leading to increased lymphocyte sequestration in lymphoid tissue via reduced $S1P_1$ surface expression. A) Pharmacological inhibition of S1P lyase increases S1P concentration in tissue. B) Reduced $S1P_1$ through shRNA increases lymphocyte sequestration in tissue and reduced lymphocytes in circulation [33].

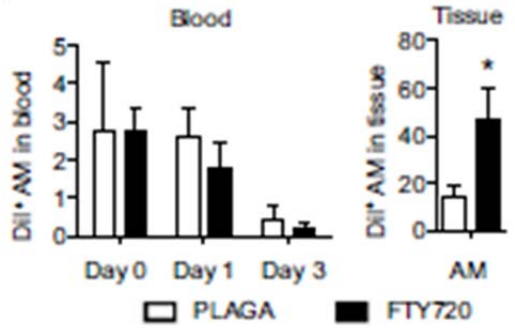

Fig 1.12: FTY720 preferentially recruits AM/M2 macrophages to the tissue from the blood in animals transplanted with DiI labeled M2 macrophages [35].

1.5 FTY720 is a Potent Agonist of $S1P_1$ and $S1P_3$

FTY720 is a small molecule drug that is an $S1P_1$ and $S1P_3$ agonist. Its status as an FDA approved oral treatment for multiple sclerosis [36], as well as its superior chemical stability and longer half-life in the body [37] compared to other growth factors makes it a desirable candidate for other clinical applications.

1.5.1 Application of FTY720 for bone regeneration and vascularization

FTY720 released from PLAGA films in a rat cranial defect has been shown to increase defect healing and smooth-muscle invested microvascular formation in a rat cranial defect (Fig 1.13) [38]. Follow up studies showed that FTY720 promoted smooth muscle cell investment onto forming vasculature, as well as improving the elastic modulus and ultimate compressive strength in a tibial defect (Fig 1.14B,C) [39]. Spatially controlled

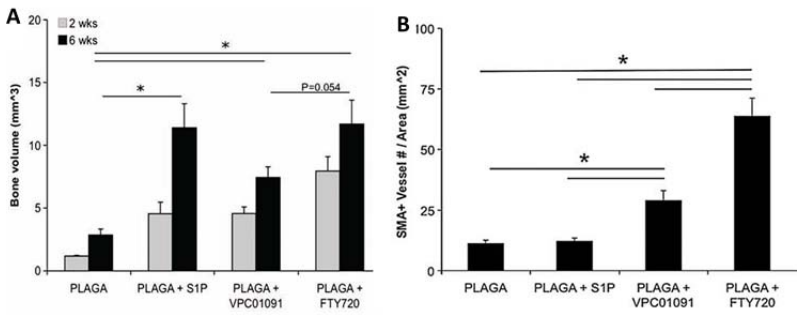

Fig 1.13: FTY720 released from PLAGA increases bone deposition and mature vasculature formation in rat cranial defect [38].

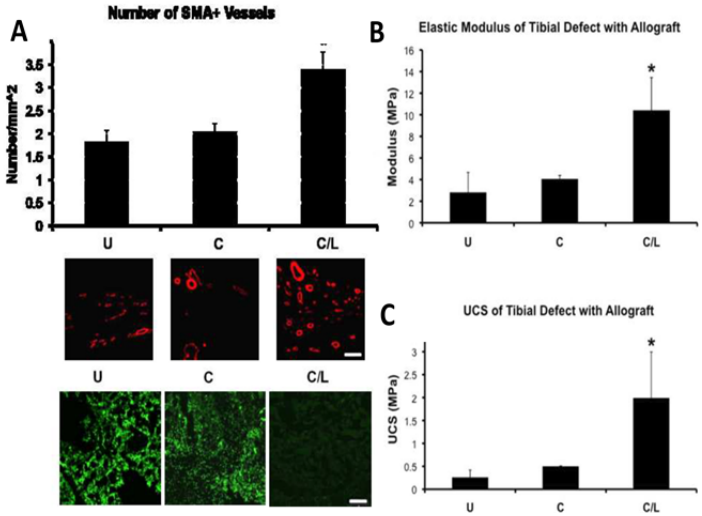

Fig 1.14: FTY720 released from PLAGA coated grafts improves vascularization and mechanical stability of the defect, and conveys local immune-suppression. A) FTY720 increases smooth muscle presences on forming vasculature as labeled by αSMA(reD). Leukocyte presence is diminished as evidences by decreased CD45 staining (green). FTY720 improves B) elastic modulus and C) ultimate compressive strength of the graft [39].

regeneration of bone within a cranial defect was achieved by FTY720 released from heterogeneously composed PLAGA microsphere scaffolds (Fig 1.15) [40]. It is evident that the defect side where the 85:15 PLAGA microspheres was located had more bone

formation compared to the 50:50 PLAGA side, confirming that polymer composition can be used to control the release rate of FTY720 in the defect . It was also demonstrated that application of FTY720 *in vivo* significantly enhanced SDF-1α mediated chemotaxis of bone marrow mononuclear cells (Fig 1.16A) [41]. FTY720 is also shown to promote BMP-2 mediated osteoblast differentiation, as evidenced by alkaline phosphatase and osteocalcin staining (Fig 1.17A,B) [42]. They also observed increased Smad 1/5/8 and ERK 1/2 phosphorylation in C2C12 cells, indicating differentiation down an osteoblastic lineage (Fig 1.17C-F) [42].

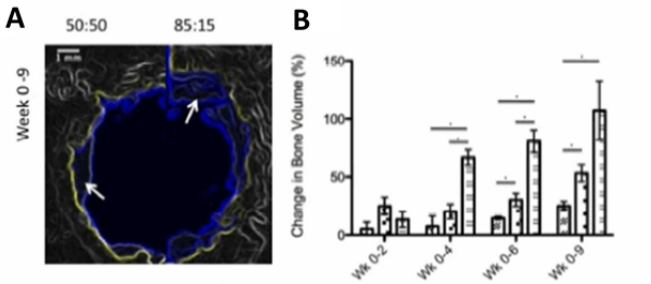

Fig 1.15: FTY720 released from heterogeneously composed PLAGA microspheres can direct bone formation. A) Composition of PLAGA influences FTY720 release rate and subsequent bone formation as quantified in B), // empty defect, ▪ 50:50 PLAGA, and = 85:15 PLAGA [40].

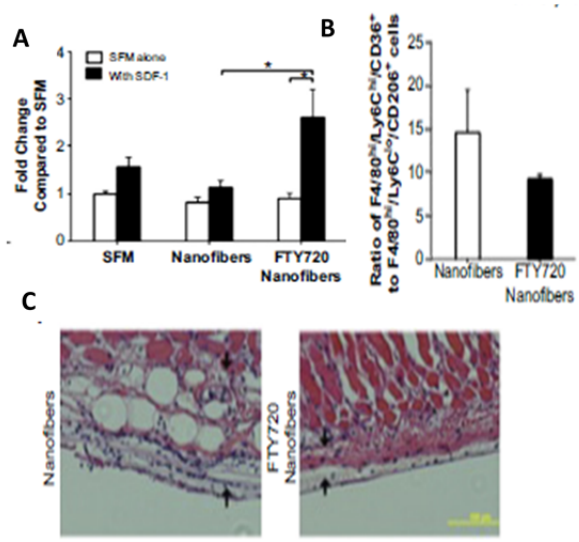

Fig 1.16: FTY720 has local immunosuppressive properties. A) FTY720 enhances bone marrow mononuclear cell chemotaxis towards SDF-1. B) FTY720 decreases the ratio of F4/80^{hi}/Ly6C^{hi}/CD36^{+} to F4/80^{hi}/Ly6C^{lo}/CD206^{+} cells as characterized by flow cytometry. C) H&E staining shows reduced fibrous capsule formation after FTY720 treatment [41].

Finally, the local release of FTY720 from PLAGA films in a dorsal skinfold window chamber produced up to a 153% increase in local microvascular length density s well as increased smooth muscle investment after 7 days (Fig 1.18A,B) [43]. Imaging of the spinotrapezius muscle on the back of a mouse after treatment with PLAGA or FTY720 shows collateral formation and increased vascular branching (Fig 1.18C,D)[43].

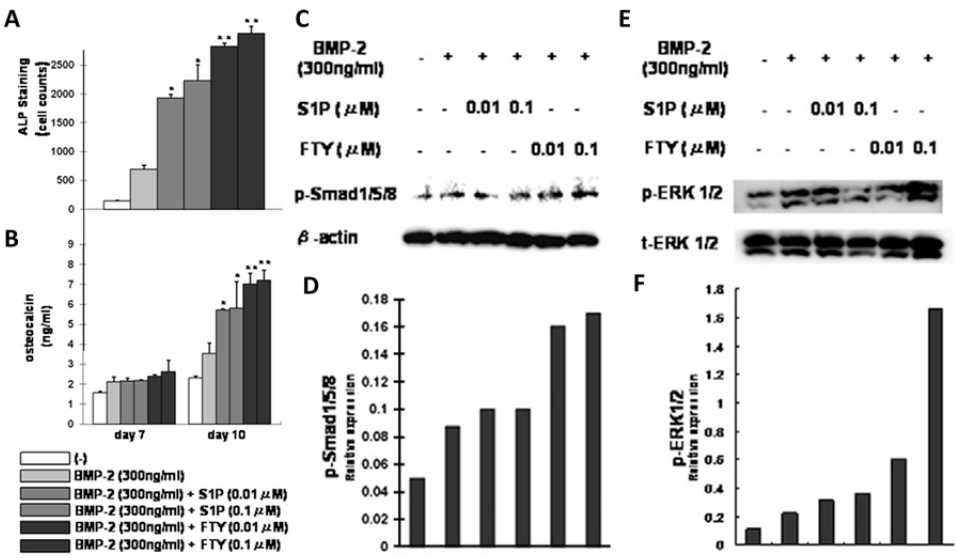

Fig 1.17: FTY720 increases osteoblast differentiation of C2C12 cells. FTY720 increases A) alkaline phosphatase (ALP) and B) osteocalcin staining, indicating increased osteoblast differentiation. FTY720 increases C) Smad 1/5/8 phosphorylation as quantified in D) and E) ERK 1/2 phosphorylation as quantified in F) [42].

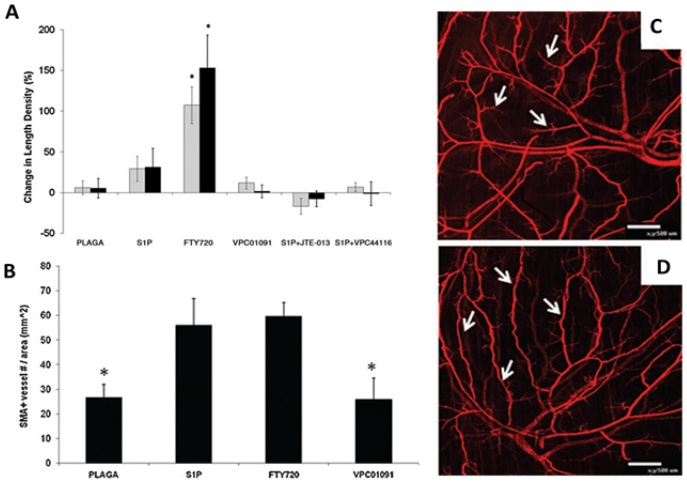

Fig 1.18: FTY720 improves arteriogenesis. FTY720 released from PLAGA films in a dorsal skinfold window chamber increases A) vascular length density and B) smooth muscle cell investment onto new vasculature. Images of spinotrapezius muscle treated with C) PLAGA and D) FTY720. Arrows indicate collateral formation [43].

1.5.2 Application of FTY720 for local immunosuppression

Successful graft integration also requires reduced immune response to the implant material. Local activation of FTY720 is shown to have immunosuppressive effects, which has been demonstrated by inhibition of lymphocyte recirculation (Fig 1.19 and Fig 1.20) [44,45].

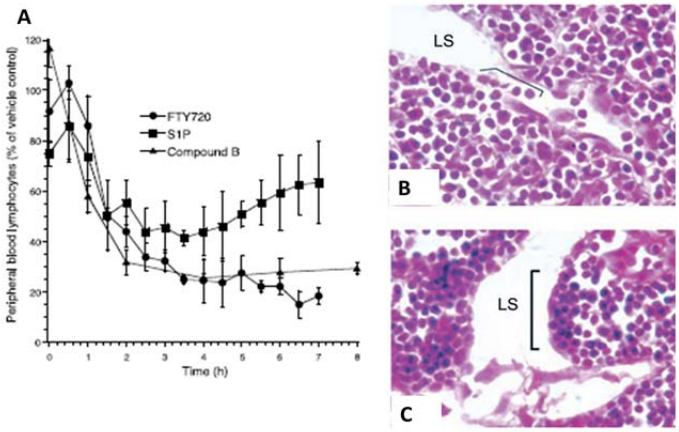

Fig 1.19: FTY720 decreases leukocytes in circulation. A) FTY720 induces rapid peripheral blood lymphopenia. Lymphocyte migration into murine sinus is decreased when treated with C) FTY720 compared to B) control. [44].

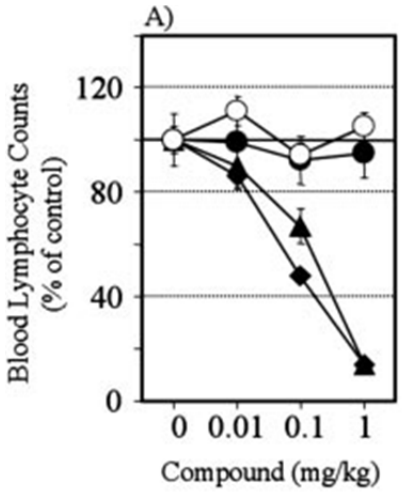

Fig 1.20: FTY720 reduces blood lymphocytes [45].

Furthermore, a decreased leukocyte presence is observed in defects that contain FTY720-releasing graft as evidenced by decreased CD45 staining (Fig 1.14A) [39]. Additionally, FTY720 release from PLAGA nanofibers in a dorsal skinfold window chamber generated a smaller fibrous capsule compared to unloaded fibers, which indicates a diminished immune response around the implant (Fig 1.16B) [41]. Subsequent application of FTY720-loaded PLAGA nanofibers into a mandibular bone defect in Sprague Dawley rats increased the recruitment of M2 anti-inflammatory, pro-regenerative macrophages ($Ly6C^{lo}CD206^{+}$ cells), promoting bone deposition in the defect (Fig 1.16C) [41]. It has been shown that FTY720 in combination with cyclosporin A improved graft survival via histological evaluation (Fig 1.21 A-D)

and by reducing $CD4^+$ and $CD8^+$ T cells in circulation ten days after graft transplantation (Fig 1.21E) [46].

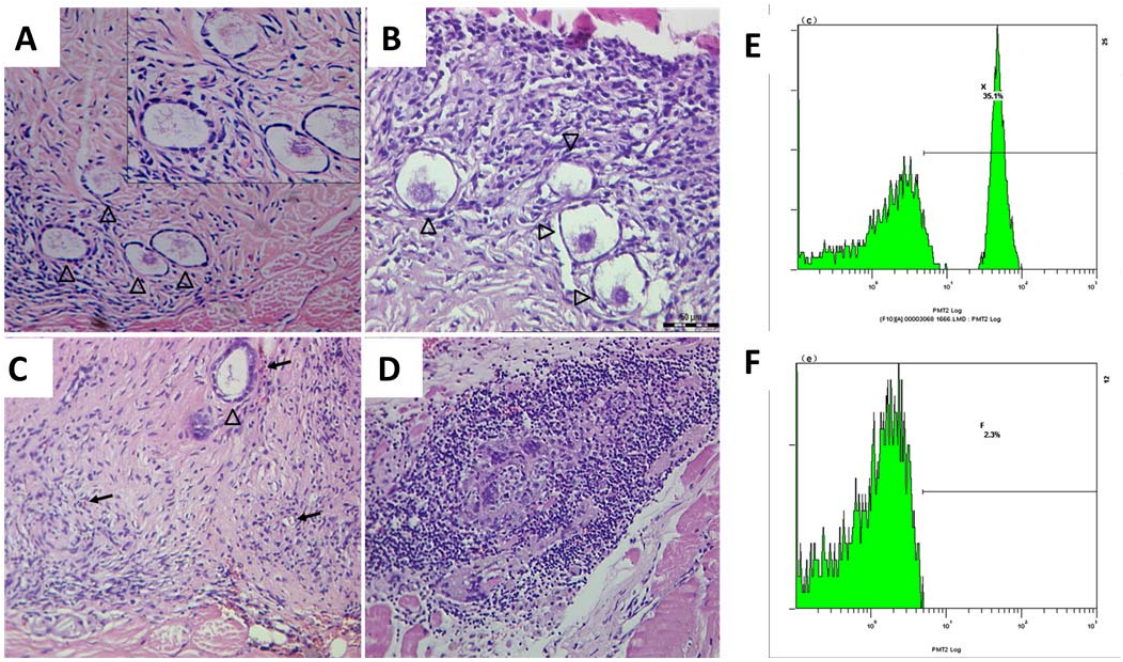

Fig 1.21: FTY720 reduces lymphocyte numbers after ovarian tissue transplantation. There is reduced infiltration of macrophages and lymphocytes into ovarian tissue with grafts treated with a-C) FTY720 and cyclosporin A compared to D) cyclosporin alone as stained by H&E. Reduced CD4/CD8 cells in peripheral blood when animal is pre-treated with FTY720+cyclosporin A on F) day 10 compared to E) day 0 as evaluated by flow cytometry [46].

The immune-protective properties of FTY720, in addition to its roles in increasing bone cell recruitment and vascularization makes it an ideal candidate for use in bone wound regeneration.

1.6 Poly(lactic co-glycolic acid) as a Biomaterial for Bone Repair

Poly (lactic-co-glycolic acid)(PLAGA) is a widely used synthetic material for medical applications due to its high biocompatibility and low immunogenicity and toxicity [47], its highly customizable physical and mechanical properties [49,50,51]**,** and its approval for use by the Food and Drug Administration (FDA) makes it a promising technology for clinically translatable applications [50]. For bone regeneration, PLAGA has been successfully used in a variety of forms to facilitate healing in animal models of

bone injury [49,51,52,53,54]. Further studies show that augmentation of synthetic materials, often with growth factors such as vascular endothelial growth factor (VEGF) [6,55,56], bone morphogenetic factor (BMP) [57,58], and others, often times improves bone regeneration within and revascularization of the defect area. Some concern over the supra-physiological doses of BMP to achieve bone healing causing undesired bone formation encourages exploration of other therapeutic agents [59]. In the past, we have used FTY720, a small molecule with agonist activity at receptors $S1P_1$, and $S1P_{3\text{-}5}$, released from scaffolds composed of PLAGA placed within critical sized bone defects to promote bone regeneration and vascularization [38,39,40,41,43,60].

Despite the many published instances of PLAGA applications in animal models, and its status as an FDA-approved material, only a very small fraction of those technologies have reached clinical trials, and only a select few of those PLAGA based medical technologies are commercially available for use to treat bone injuries, or for drug or cell delivery. A survey of PLGA based technologies in clinical trials include a bone graft by ISTO Technologies composed of PLGA/hyaluronic acid and bone,[61,62,63], and a resorbable bone screw that releases ciprofloxacin and performs superior to titanium screws in preventing bacterial infection [64]. Boston Scientific Corporation has an ongoing phase III clinical trial for a coronary stent partially composed of PLAGA, called the Synergy [65,66,67], and preliminary study results indicate successful drug elution from the stent over the course of 30 days . Yet this is a very small number of clinical trial studies compared to the number of published PLAGA-containing implant technologies that are developed and tested in animal models.

One potential concern is that nanoscale PLAGA-based delivery vehicles accumulate preferentially in the liver, which may cause toxicity [47]. Furthermore, empty PLAGA nanoparticle administration to Balb C mice to evaluate blood-brain barrier permeability appeared to cause otherwise unexplained sedation and pain to the animals [68]. However, nanoscale particles convey desirable targeted drug delivery

characteristics by being more invisible to the immune system. Additionally, the widely tunable drug release kinetics and mechanical properties may require further characterization and testing before use in human subjects [69].

1.7 Specific Aims Addressed in this Thesis Project

The studies presented in this thesis set forth to address two specific aims.

1.7.1 Evaluating the efficacy of topically applied FTY720 for bone regeneration in a sub-critical tibial defect

FTY720 has been incorporated previously in PLAGA coatings of bone allografts, and was shown to promote bone regeneration. *Objective 1* of this aim is to develop a local delivery system for FTY720 in a tibial defect model. The delivery vehicle of choice is a polymer plug composed of Matrigel, a basement membrane-derived polymer. *Objective 2* of this aim is to use the delivery system from objective 1 in an animal model of a long bone defect, specifically in the tibia of a mouse. The development of this model would be valuable in allowing future use of transgenic mouse models to more closely interrogate different processes and cell functions involved in wound repair that are less feasible in rat models of tibial defects. The efficacy of the FTY720 treatment will be evaluated using X-ray imaging as well as uCT imaging to measure bone regeneration.

1.7.2 Evaluating the efficacy of FTY720 adsorbed directly to the surface of a human bone allograft for bone regeneration in a critical sized cranial defect

Previous work has released FTY720 from a PLAGA-coated bone allograft to promote bone regeneration and vascularization in the defect area. *Objective 1* of this aim will be to develop and implement a PLAGA-free strategy to apply FTY720 to bone grafts. This will be accomplished by quantifying the release and activity of FTY720 from a bone graft using HPLC/MS. *Objective 2* of this aim is to apply the polymer-free bone graft developed in objective 1 into a critical size cranial defect created in Sprague Dawley rats.

uCT imaging and analysis will be employed to measure bone formation and vascularization. *Objective 3* will evaluate the tissue composition and the immune response to the bone allograft through immunohistochemical staining of harvested tissue.

1.8 Organization of Thesis

Several studies were conducted to evaluate the efficacy of locally delivered FTY720 on promoting bone regeneration and graft integration in defect models. Chapter 2 describes both the in vitro methods, the animal models used, and the methods of analysis employed to evaluate bone regeneration and vascularization. Chapter 3 will present the results and discussion obtained from the various studies performed in Chapter 2.

CHAPTER 2

METHODS

Several in vitro and in vivo models were used to evaluate the efficacy of locally delivered FTY720 on promoting bone regeneration and graft integration.

2.1 Locally Applied FTY720 Accelerates Healing of Critical Size Cranial Defect

We have previously published that local delivery of FTY720 via PLAGA degradation from a bone allograft in a rat critical size cranial defect accelerated graft integration compared to unloaded grafts [60]. The defect used to evaluate healing was circular in shape, and a semi-circular implant was placed in one half of the defect space. This model allowed us to evaluate both host-graft bridging on the graft side, as well as directed bone growth from the host bone towards the graft in the void space (Fig 2.1). This model was employed to evaluate bone deposition and vascularization over weeks. The methods below are summarized from Huang et.al. [60].

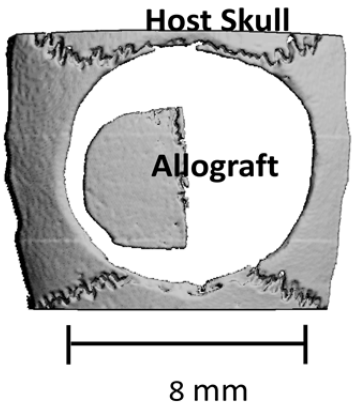

Fig 2.1: Schematic of critical size cranial defect model. Semicircular graft within the circular defect allows evaluation of host-graft bridging on the graft side, as well as new bone deposition in the void space.

2.1.1 Evaluation of FTY720 release from PLAGA and FTY720 bioactivity

FTY720 and 50:50 PLAGA polymer were dissolved into 1:12 (w/w) dichloromethane. Cranial allografts were harvested from Sprague Dawley rats and were placed in the drug: polymer solution for 10 minutes to allow a coating to form. Subsequently, the grafts

lyophilized to remove residual solvent. To measure encapsulation efficiency, the coated grafts were sonicated in chloroform to dissolve the PLAGA layer. The samples were taken through sphingolipid extraction. Briefly, D-*erythro*-Sphingosine (C-17 base) is added to the dissolved PLAGA and the solution is dried to a solid using nitrogen flow. Immediately prior to HPLC/MS analysis, this pellet was dissolved in methanol. To measure FTY720 release, the grafts were placed in vials of SBF (pH 7.2; 7.996g NaCl, 0.35g $NaHCO_3$, 0.3g KCl, 0.136g KH_2PO_4, 0.095g $MgCl_2$, 0.278g $CaCl_2$, 0.06g $MgSO_4$ in 1L deionized water). The grafts were moved into clean vials of SBF daily, and the solution from the previous day was kept for sphingolipid extraction and HPLC/MS.

Additionally, the bioactivity of the released FTY720 was validated using a sphingosine kinase 2 (SPK2) assay developed by our collaborators in Dr. Kevin Lynch's lab at the University of Virginia. It is reported that SPK2 phosphorylates FTY720 into its active form FTY720-P *in vivo* [60]. The *in vitro* assay uses purified SPK2 and a radiolabeled ^{32}P-ATP to determine of SPK2 would phosphorylate the FTY720 released from the PLAGA coating. This was measured in a Beckman Coulter LS 6500 liquid scintillation counter.

2.1.2 Creation of critical size cranial defect implanted with PLAGA-coated graft

Animals received either graft with no PLAGA coating (uncoated), a graft with PLAGA coating (coated), a graft coated 1:200 w/w FTY720:PLAGA (low FTY720) or a graft coated with 1:40 w/w FTY720:PLAGA (high FTY720). Briefly, the dorsal skin was sterilized and a longitudinal incision was made over the dorsum of the skull over the sagittal suture through the skin and periosteum. The periosteum was elevated and reflected laterally. A 3mm round burr was used to create a 9mm defect in the bone under constant saline irrigation using a Hall High Speed Drill (CONMED, Linvatec, Largo, FL). The semicircular graft was placed underneath the periosteum, in direct contact with the parietal bone, centered on the sagittal suture and between the coronal and lamboid

sutures. The periosteum and skin were sutured shut, and animals were given Ketoprofen (3mg/kg SC) for three days post surgery to minimize pain. Rats were given free access to food and water, and were monitored for complications or abnormalities.

At each time point, animals were placed in the uCT and scanned in air with the following parameters: 38 μm voxel size, 55 kVp, 145 μA, medium resolution, 38.9 mm diameter field of view, and 200 ms integration time (73 mGy radiation per scan). The threshold for bone evaluation was set at 481.3mg hydroxyapatite (HA)/cm^3. Each animal's scans maintained the same number of slices (≈260 slices) for the entire study, centered at the defect, with equal extension in the anterior and posterior directions from the edges of the defect. Regions of interest were drawn on the 2D image slice, and were bounded by the physiological ridges that separate the parietal bone from the temporal bone, resulting in the inclusion of all the parietal bone through the slices.

2.1.3 MICROFIL perfusion of wound area for uCT evaluation

At week 8, after uCT imaging for bone growth, cranial blood vessels were perfused with MICROFIL, a radio-opaque solution, to allow for imaging and quantification of vessel growth by uCT. Briefly, the rats were euthanized and the heart was exposed. The common carotid arteries were cannulated, and a small incision was made in the right atrium of the heart to allow blood drainage. The arteries were then ligated directly beneath the cannulation points to allow perfusion of the head region with a heparin-saline solution to push the blood out of circulation. Then, 3mL of MICROFIL was perfused from each artery over 5 minutes. The solution was allowed to set for 16 hours at 4°C, after which the area surrounding the parietal bone was harvested, fixed and decalcified. Following decalcification, samples were scanned in are with the following parameters: 21μm, 45kVp, 177μA, medium resolution, 21.5 mm diameter field of view and 200ms integration time. Vasculature was thresholded from decalficied tissue using 164-1500

HA/cm^3 and the sagittal sinus was excluded from analysis due to its large and varying size between animals.

2.2 Locally Applied FTY720 for Graft Integration in Chimeric Tibial Defect

While cranial size critical defects are supremely useful for investigating bone defects in a non-load bearing environment such for craniofacial applications, it was also important to evaluate how FTY720 treatment improves graft integration in load bearing injuries. We are also interested in the origin of the various cells that contribute to the wound healing process. In order to begin addressing these questions, we use a tibial defect model created in chimeric eGFP Sprague Dawley rats to probe the source of cells that contribute to wound healing, while also investigating the mechanical integrity of the FTY720-treated graft.

2.2.1 Creation of tibial defect implanted with PLAGA graft

Rats were lethally irradiated with 10 grays over 2 hours to deplete their native bone marrow. Subsequently, bone marrow harvested from eGFP rats was transplanted into the irradiated rats and allowed to engraft over 5 weeks, as shown in Fig 2.2. In this manner, all future cells that come from the bone marrow would constitutively express GFP,

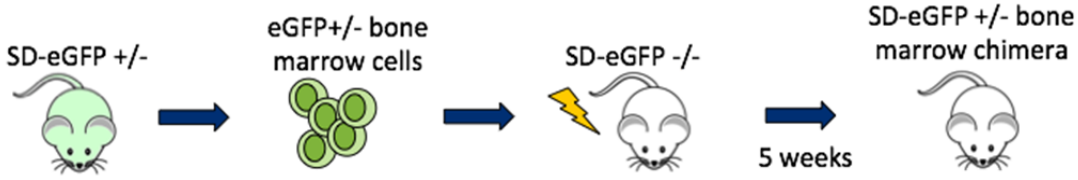

Fig 2.2: Schematic for eGFP chimeric rat creation on a Sprague Dawley background.

allowing us to monitor the source of cells contributing to regeneration in the defect.

Segmental tibial defects were surgically created in the right hind limb of each eGFP chimera. Rats were given one of three treatments in the right hind limb: allograft alone (c), PLAGA-coated allograft (p), and PLAGA-coated allograft containing FTY720 (d). Wounds were allowed to heal for 12 weeks.

2.2.2 Mechanical testing of rat tibia

After twelve weeks, both the unfractured left hind limb, which served as the contralateral control, and the experimental right hind limb were harvested for mechanical evaluation. Using a Bose Endura TEC ELF 3220 system, the distal end of the tibia was held in a fixed position, while a constant rotation of 3°/second was applied to the proximal end of the tibia until the bone fractured. The maximum torsional force was recorded, as well as the rotation of the proximal end at failure. It was observed that all graft failures occurred at the interface of the graft and host bone.

2.2.3 Histological evaluation of tissue

Tissue was harvested from the wound area at 12 weeks. Sections were stained with GFP and CD90 to determine whether CD90+ progenitor cells were also positive for GFP. Co-staining indicated the recruited cells originated in the bone marrow.

2.3 Topically Applied FTY720 for Bone Regeneration in a Sub-Critical Tibial Defect

Here, we describe a sub-critical tibial defect model that was developed in mice, which we hope will allow us to take advantage of the various opportunities to create transgenic mouse models that would allow closer inspection of cellular processes involved in wound healing that are not feasible in rat models. This thesis will describe the model, as well as the development of a strategy to locally deliver an injectable, FTY720-loaded vehicle into a sub-critical tibial defect where no bone graft is used. Without a bone graft in place, the cues provided by the mineralized matrix are removed, and any mechanical support provided by the graft scaffold is removed as well. Instead, we inject a viscous Matrigel plug loaded with FTY720, which then hardens at body temperature.

2.3.1 Creation of tibial defect

A tibial defect was created in Balb/C mice using a Bonnerans-Einhorn device, pictured in Fig 2.3. Briefly, an incision was made over the knee, and a sterile metal pin was inserted into the medullary canal. Mice were placed on the holder of the Bonnerans-Einhoren device, and a 220g weight was dropped from a height of 40cm onto a blunt blade in contact with the tibia. 0.1mL of Matrigel was injected into the defect area of each animal. Animals were sorted into three groups: 1) no drug, 2) 1nM FTY720 (low) in Matrigel, and 3) 10nM FTY720 (high) in Matrigel. The Matrigel was viscous as room temperature, and hardened into solid plugs at body temperature.

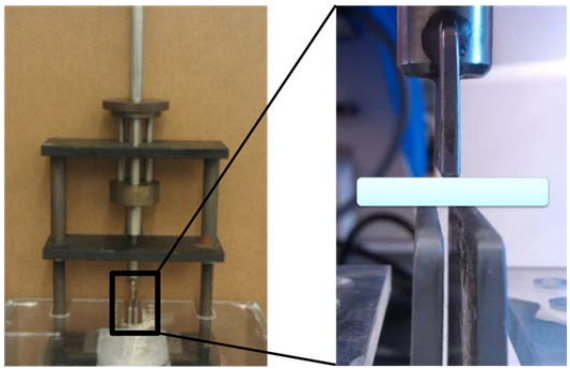

Fig 2.3: Description of the Bonnarens-Einhoren device. The white specimen in the right panel represents the mouse tibia.

The metal pin inserted into the medullary canal interfered with the uCT imaging, so therefore two methods were employed to image the tibial defects. Every week, all mice were imaged by X-ray, using a 1 minute exposure time at 30eV. At each time point, some animals were euthanized and the hind limbs were harvested. The pin was removed, and the limbs were imaged by uCT in air using medium resolution and voxel dimensions of 0.21μm.

2.4 Locally Applied FTY720 Adsorbed Directly to Surface of Human Bone Graft in Critical Size Cranial Defect

FTY720 has been described to have immunosuppressive properties when applied locally. To investigate this in a bone defect environment, as well as the evaluate the potential to eliminate the polymer phase in the drug delivery vehicle, we directly adsorb FTY720 to the surface of a human bone graft and implant it into a critical size cranial defect created in rats.

2.4.1 FTY720 drug loading onto and release from human trabecular allograft

Human trabecular grafts were received from collaborators at Lifenet Health. The grafts were washed in their proprietary Allograft XG to remove cellular debris. FTY720 was fully dissolved into methanol, and the graft was placed inside to allow drug to adsorb. To measure loading efficiency, the pre- and post-loading methanol solution was saved for sphingolipid extraction. Briefly, D-*erythro*-Sphingosine (C-17 base) is added to the dissolved PLAGA and the solution is dried to a solid using nitrogen flow. Immediately prior to HPLC/MS analysis, this pellet was dissolved in methanol. To measure FTY720 release, the grafts were placed in vials of SBF (pH 7.2; 7.996g NaCl, 0.35g $NaHCO_3$, 0.3g KCl, 0.136g KH_2PO_4, 0.095g $MgCl_2$, 0.278g $CaCl_2$, 0.06g $MgSO_4$ in 1L deionized water). The grafts were moved into clean vials of SBF daily, and the solution from the previous day was kept for sphingolipid extraction and HPLC/MS.

2.4.2 Creation of critical size cranial defect

Female Sprague-Dawley rats (6-8 weeks) underwent a critical size (8mm) defect surgery, as illustrated in Fig 2.1. Briefly, the dorsal skin was sterilized and a longitudinal incision was made over the dorsum of the skull over the sagittal suture through the skin and periosteum. The periosteum was elevated and reflected laterally. A 3mm round burr was used to create a 9mm defect in the bone under constant saline irrigation using a Hall High Speed Drill (CONMED, Linvatec, Largo, FL). The semicircular graft was placed underneath the periosteum, in direct contact with the parietal bone, centered on the sagittal suture and between the coronal and lamboid sutures, and the periosteum and skin were sutured shut.

The animals received one of three treatments (n=6): no implant, human trabecular semicircular bone graft (graft-only), and FTY720-loaded human trabecular semicircular bone graft (graft + FTY720). The FTY720 was adsorbed directly to the bone grafts as

previously described. The grafts were analyzed and distributed evenly among the two graft groups to control for graft size and density variation.

uCT will be used to evaluate bone formation every two weeks. Briefly, rats were imaged in air using the following parameters: 38 μm voxel size, 55 kVp, 145 μA, medium resolution, 38.9 mm diameter field of view, and 200 ms integration time (73 mGy radiation per scan). The threshold for bone evaluation was set at 481.3mg hydroxyapatite (HA)/cm^3. Each animal's scans maintained the same number of slices (≈260 slices) for the entire study, centered at the defect, with equal extension in the anterior and posterior directions from the edges of the defect. Regions of interest were drawn on the 2D image slices. In the cranial defect, the region of interest was bounded by the physiological ridges that separate the parietal bone from the temporal bone, resulting in the inclusion of all the parietal bone through the slices.

2.4.3 MICROFIL perfusion of wound area for uCT evaluation

uCT will also be used to evaluate vascularization of the defect region. At weeks 2 and 12, after *in vivo* imaging for bone formation, animals will be euthanized for the purposes of vascular visualization in the microCT. Briefly, the common carotid arteries will be cannulated. The vasculature will be flushed with 10 mL 2% heparin-saline, then filled with 3 mL MICROFIL© injected simultaneously through both arteries, and allowed to set for 16h at 4°C. The top of the skull will be harvested, fixed, and decalcified. The following microCT parameters were used previously to scan the microvasculature in air: 21 μm voxel size, 45 kVp, 177 μA, medium resolution, 21.5 mm diameter field of view, 200 ms integration time, and threshold of 164-1500 mg HA/cm^3. Similar to bone analysis, 2D contours will be drawn to enclose the area of interest, excluding the sagittal sinus because of its large volume compared to other microvasculature, and due to the large variance of its size between samples. Additionally, this analysis will be split along

the sagittal sinus to allow comparison between vasculature in the empty defect space (void side) and the side containing the graft (graft side).

2.4.4 Histological evaluation of tissue

At the final timepoint tissue sections were taken for histological analysis. Sections were stained for Hematoxylin & Eosin, as well as Massons Trichrome to evaluate tissue composition. Additional immunohistochemical and immunofluorescence staining was performed using CD90 to label osteoprogenitor cells, CD29 to detect bone marrow stromal cells, CD68 to detect macrophages, and CD34 to label endothelial cells.

CHAPTER 3

RESULTS

3.1 Locally Applied FTY720 Accelerates Healing of Critical Size Cranial Defect

As described in Chapter 2, a critical size cranial defect was employed to evaluate the effect of locally released FTY720 from a PLAGA-coated bone allograft on bone regeneration and vascularization.

3.1.1 FTY720 release from PLAGA coating maintains bioactivity

We showed that about 50% of the total loaded FTY720 was released into the SBF, and the activity profile indicates that the FTY720 released from the graft could be phosphorylated by SPK2 (Fig 3.1) [60]. Drug release is governed by PLAGA degradation from the graft, and the entirety of the PLAGA coating would be expected to degrade over 4-8 weeks [61], over which FTY720 should remain bioactive.

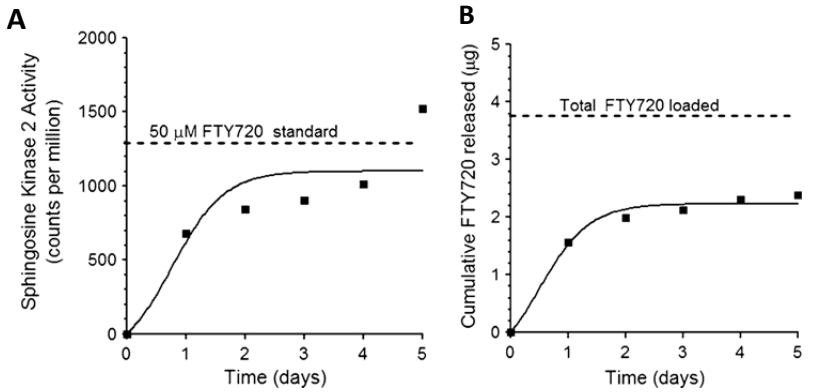

Fig 3.1: FTY720 A) bioactivity and B) release from PLAGA-coated grafts in simulated body fluid as evaluated by a SPK2 activity assay and HPLC/MS [60].

3.1.2 FTY720 promotes total bone growth

FTY720 treated groups showed almost complete graft-host integration on the graft side of the defect, as well as directed bone growth within the void space (Fig 3.2A) [60]. Bi-weekly quantification of bone growth revealed that the higher dose FTY720 accelerated new bone formation in the first two weeks, but by 8 weeks both the low and high dose FTY720 groups exhibited similar levels of total bone formation (Fig 3.2B).

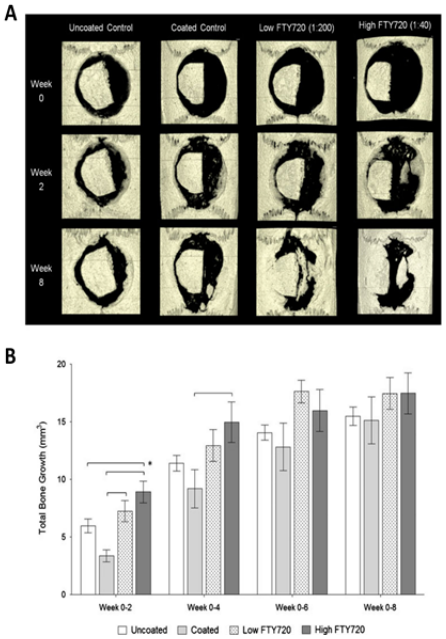

Fig 3.2: FTY720 promotes bone regeneration in rat cranial defect. A) Time-lapse uCT reconstructions of cranial defects. B) Quantification of bone deposition by uCT over 8 weeks [60].

3.1.3 FTY720 promotes graft integration through vascularization

FTY720 did not have a significant effect on increasing total vessel growth. However, we observed that the control groups had particularly poor vessel infiltration into the graft, but the FTY720 groups show vessel formation in the plane of the graft and periosteum. When quantifying vessel growth either from

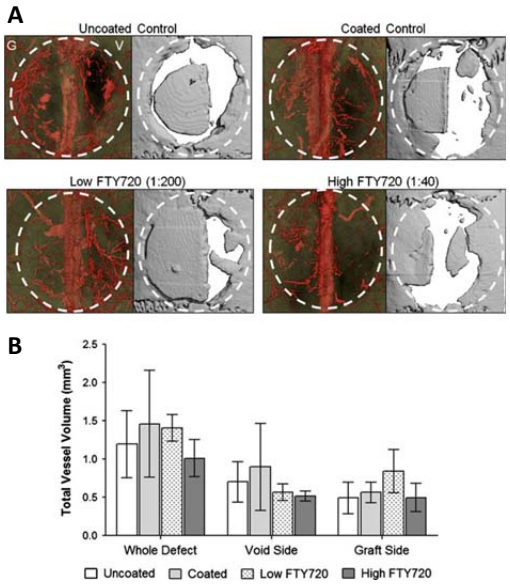

Fig 3.3: FTY720 increases vascularization on the graft side of the defect. A) Side-by-side visualizations of bone formation and vascular growth as imaged by MicroCT. B) Quantification of vascular growth via MICROFIL-assisted MicroCT. The FTY720 treated groups experience more vascular penetration on the graft side compared to unloaded and uncoated controls [60].

MICROFIL-assisted uCT analysis, or from assessment of αSMA histology of cranial tissue sections for smooth muscle investment around vasculature, the total amount of vessel growth was not significantly different between groups at week 8 (Fig 3.3). However, the FTY720 treated groups appear to have improved blood vessel investment into the graft.

3.2 Locally Applied FTY720 for Graft Integration in Chimeric Tibial Defect

As described in chapter 2, an eGFP chimeric rat was created to evaluate the origin of cells recruited to the tibial defect. Firstly a differentiation assay was used to confirm the multipotency of cells in the chimeric bone marrow, as shown in Fig 3.4. With this confirmation, we were able to use the chimeric rat model to evaluate the origin of cells recruited to the defect area to participate in wound healing.

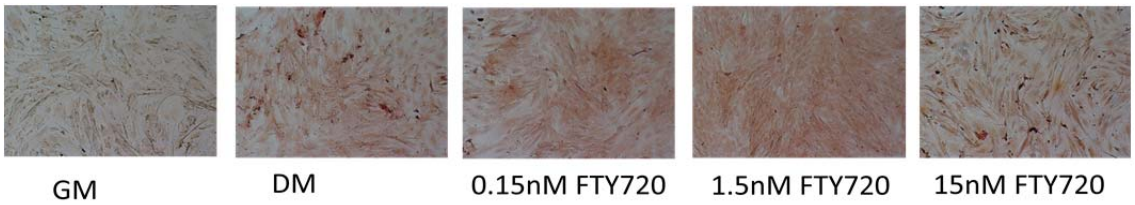

Fig 3.4: Bone marrow cells harvested from chimeric eGFP rats differentiate down osteogenic lineage. Alizarin red staining increases with FTY720 dose, independent of cell seeding density.

3.2.1 FTY720 increases mechanical strength of soft tissue

We observe that FTY720 released from PLAGA increases soft tissue toughness by 6 times compared to the unfractured contralateral control in the untreated group (control c)(Fig 3.5B). Additionally, the bone could withstand more rotation before failure as compared to control c (Fig 3.5B). The toughness of the bone itself remained unchanged across all groups. We have previously observed that application of FTY72 increases vascularization in the graft [60]; this may be anchoring the graft more firmly into the defect space compared to unloaded graft, which is contributing to the higher rotation required to induce graft failure. The higher soft tissue toughness could be attributed to

higher amounts of soft tissue formed around the graft interface. It has been shown that FTY720 increases osteoblast differentiation; it is possible that the increased osteoblast presence leads to increased deposition of collagen that has not been remodeled into mature bone. Reports show that collagen fibers are more elastic compared to mineralized bone, so it would make sense that the more pliable soft tissue is more plastic compared to mineralized bone [71].

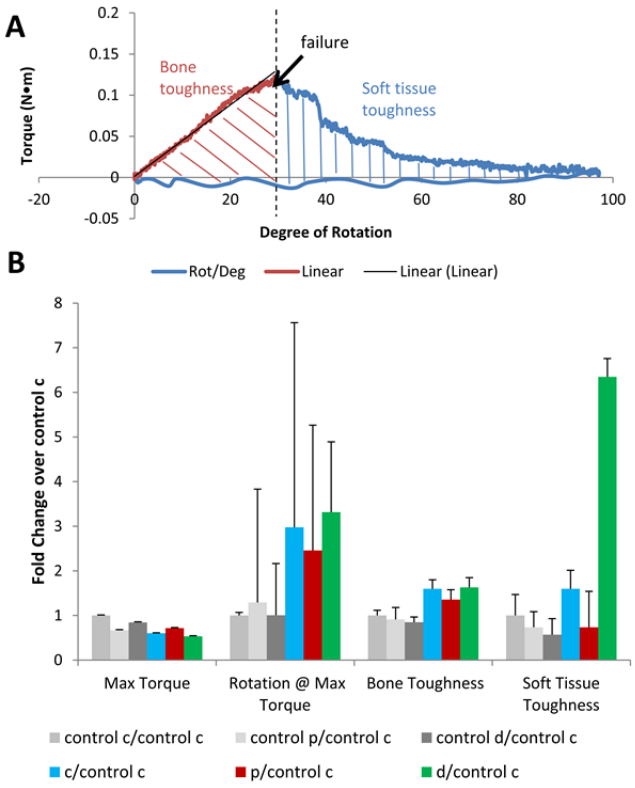

Fig 3.5: FTY720 improves mechanical integrity of graft in a tibial defect in rats. A) sample analysis of a data point. B) Comparison of max torque, rotation, bone toughness and soft tissue toughness in empty graft (c), PLAGA graft alone (p) and PLAGA graft + FTY720 (d).

3.2.2 FTY720 increases recruitment of progenitor cells from the bone marrow

Histological staining was performed to determine the origin of cells recruited to the defect area. Analysis revealed that in groups treated with FTY720, there was an increased presence of eGFP+ CD90+

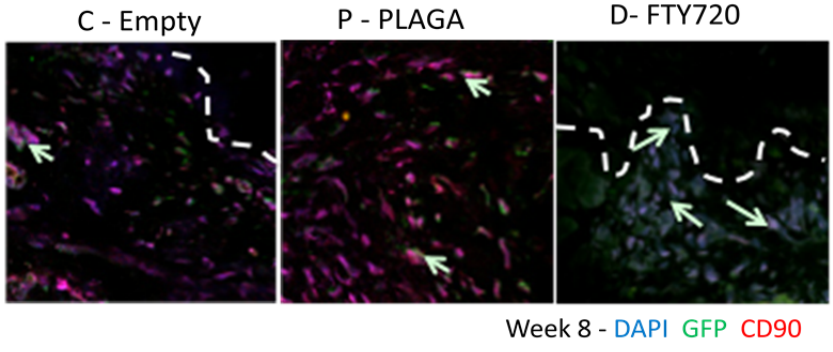

Fig 3.6: FTY720 increases recruitment of CD90+ cells from the bone marrow. The edge of the graft is outlined. Arrows indicate cells that are positive for GFP and CD90.

osteoprogenitor cells compared to untreated and PLAGA only groups (Fig 3.6). Additionally, it appears that the eGFP+CD90+ cells are infiltrating the graft area as indicated by the dotted line (Fig3.6). Cells that are labeled gray are cells that are positive for both markers, indicating they came from the bone marrow.

3.3 Topically Applied FTY720 for Bone Regeneration in a Sub-Critical Tibial Defect

A large number of bone defects are not suited for implantation of a bone graft. Additionally, non-union healing occurs in about 10% of the 7.9 million annual bone fracture incidences [72]. To that end, we set out to develop an injectable, graft free strategy using freely diffusing FTY720 to promote healing in sub-critical tibial defects. It can be seen that at two weeks, FTY720 appears to accelerate the increase of bone volume in the defect area, though by four weeks all four groups appear to have the same bone volume (Fig 3.7A). FTY720 appears to accelerate the formation of the fracture callous, as evidenced by the decrease in bone density of the FTY720 groups at two weeks (Fig 3.7B). The bone density rises by four weeks as the fracture callous is remodeled, which can be seen in the X-rays in Fig 3.7A. It is established that fracture healing in particular occurs in two general phases: first, a bony callous is formed to provide temporary mechanical stability to the defect, then cells migrate into the defect area to remodel the callous and deposit more mineral to achieve cortical union between the two ends of the defect [73,74]. The application of FTY720 appears to accelerate the formation of the fracture callous, and the uCT reconstructions in Fig 3.7B indicate that the treated groups achieved cortical union at four weeks whereas the untreated group did not. It has been shown that FTY720 enhances BMP-2 mediated osteoblast differentiation [42] and that FTY720 significantly enhances SDF-1α mediated chemotaxis of bone marrow mononuclear cells [41], both of which likely contribute osteogenic cells to deposit and remodel the fracture callous.

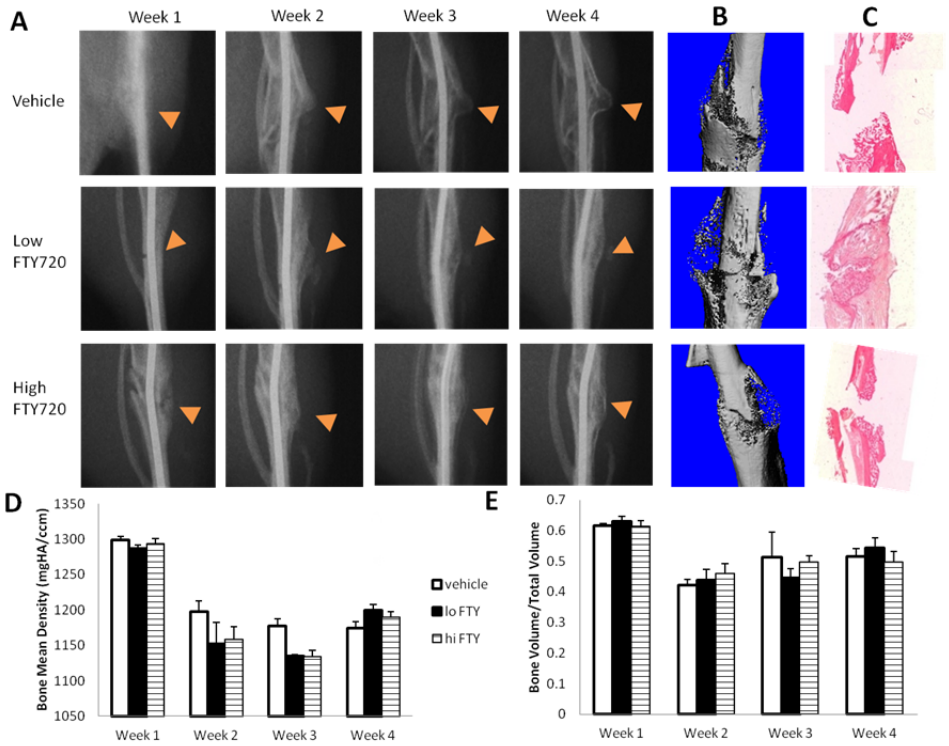

Fig 3.7: FTY720 released from Matrigel accelerates callous remodeling in mouse tibial defect. A) Xray images of defect healing and callous remodeling over 4 weeks. Arrow indicates location of fracture and callous. B) uCT reconstruction of excised tibia after four weeks. C) H&E staining of excised tibia after four weeks. D) Bone mean density and E) bone volume/total volume evaluated by uCT in the mouse tibial defect.

3.4 Locally Applied FTY720 Adsorbed Directly to Surface of Human Bone Graft in Critical Size Cranial Defect

3.4.1 Sustained released of FTY720 directly adsorbed to human trabecular bone continues over 4 weeks

As described, FTY720 was adsorbed directly to the surface of human trabecular bone grafts. Quantification of pre- and post-loading solutions showed an average drug loading of 193ug FTY720/mm^3 bone graft, with a loading efficiency of 90% (Fig 3.8A). FTY720 release is sustained over four weeks, with a burst release in the first three days followed by slower release. This burst release could be attributed to the fast release of FTY720

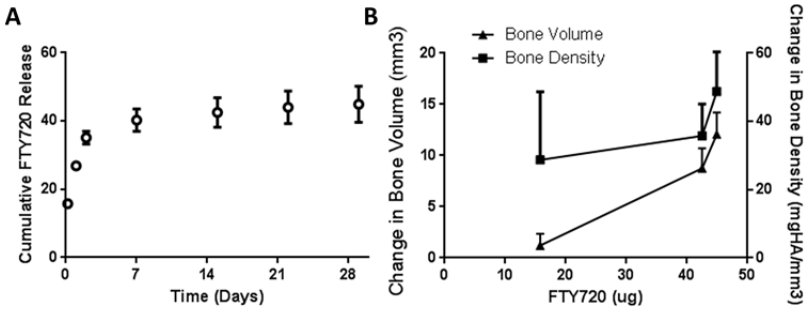

Fig 3.8: FTY720 release from human bone allograft. A) FTY720 release is sustained over 28 days. B) Bone volume and bone density increase with increased FTY720 release.

from the surface of the bone graft, and the linear profile suggests this release is limited by diffusion from the surface. The continued release could be attributed to the release of FTY720 from the bulk mass of the graft. Previous incarnations of this graft used a PLAGA coating to load FTY720 to the bone allograft, and saw a 10-fold lower loading efficiency (Fig 3.1B). FTY720 loading efficiency was limited by the dissolution of FTY720 in the PLAGA solution, whereas here FTY720 loading efficiency is only dependent on the surface area of the graft itself, as well as the drug molecule's ability to bind to itself. While drug release was driven by PLAGA degradation in the PLAGA-coated graft, here it is driven by direct diffusion off the surface of the graft into the defect environment.

3.4.2 Local release of FTY720 from human trabecular bone facilitates increased graft integration over 12 weeks

Bone deposition was evaluated bi-weekly using uCT analysis. As shown in Fig 3.9A, FTY720 increases bone regeneration, both in bridging the graft to the edge of the defect, as well as depositing bone in the void space. Bone volume is shown to increase with increasing release of FTY720 from the graft, as shown in Fig 3.9D, and bone volume is consistently higher in defects treated with FTY720 compared to grafts without. In addition to a positive linear correlation between drug release and bone volume increase, there is a steeper increase in bone volume when at least 40ug of FTY720 has been

released (Fig3.8B), suggesting there may be an optimal dose for accelerated bone formation at the higher drug dose. It also appears that bone deposition may occur preferentially within the void space; we observe that while bone volume steadily increases over 12 weeks, bone density experiences a downturn after week 10 (Fig 3.9 B,D). Newly formed bone that is deposited in the void space would likely be less dense compared to mineral deposition within the graft structure itself.

Huang et.al. observed an overall higher magnitude of bone growth in the cranial defect, but also observed a smaller amount of released FTY720 [60]. It is possible that although FTY720 promotes bone regeneration and vascularization, there is a saturation limit for FTY720, and once reached, there is no further augmentation of wound repair. The new results presented here could inform a maximum required dose to achieve graft integration, and therefore potential costs of therapy could be reduced by lowering the necessary drug loading.

Representative uCT images of MICROFIL perfused animals show vascularization within the defect area (Fig 3.10A). Specifically, we observe increased vascularization on the graft side compared to the void side, suggesting improved integration of the graft with the host bone (Fig 3.10B), which would improve the overall lifetime of the implant in the defect area.

It is well documented that integration of the graft with the host is necessary for healing to occur, both through neovascularization and bone graft resorption [22, 75]. In clinical trial using an rh-BMP2 releasing sponges in human tibial fractures, 23% of the human subjects experienced treatment failure due to lack of graft integration [76]. Previous work has shown that FTY720 promotes increases vascular diameter expansion and length density when locally applied in a mouse dorsal skinfold window chamber [43, 77], and within cranial defect models [38,60**]**. Here, we show that FTY720 facilitates higher vascularization within the graft compared to in the void space, indicating increased graft integration with the host bone**.**

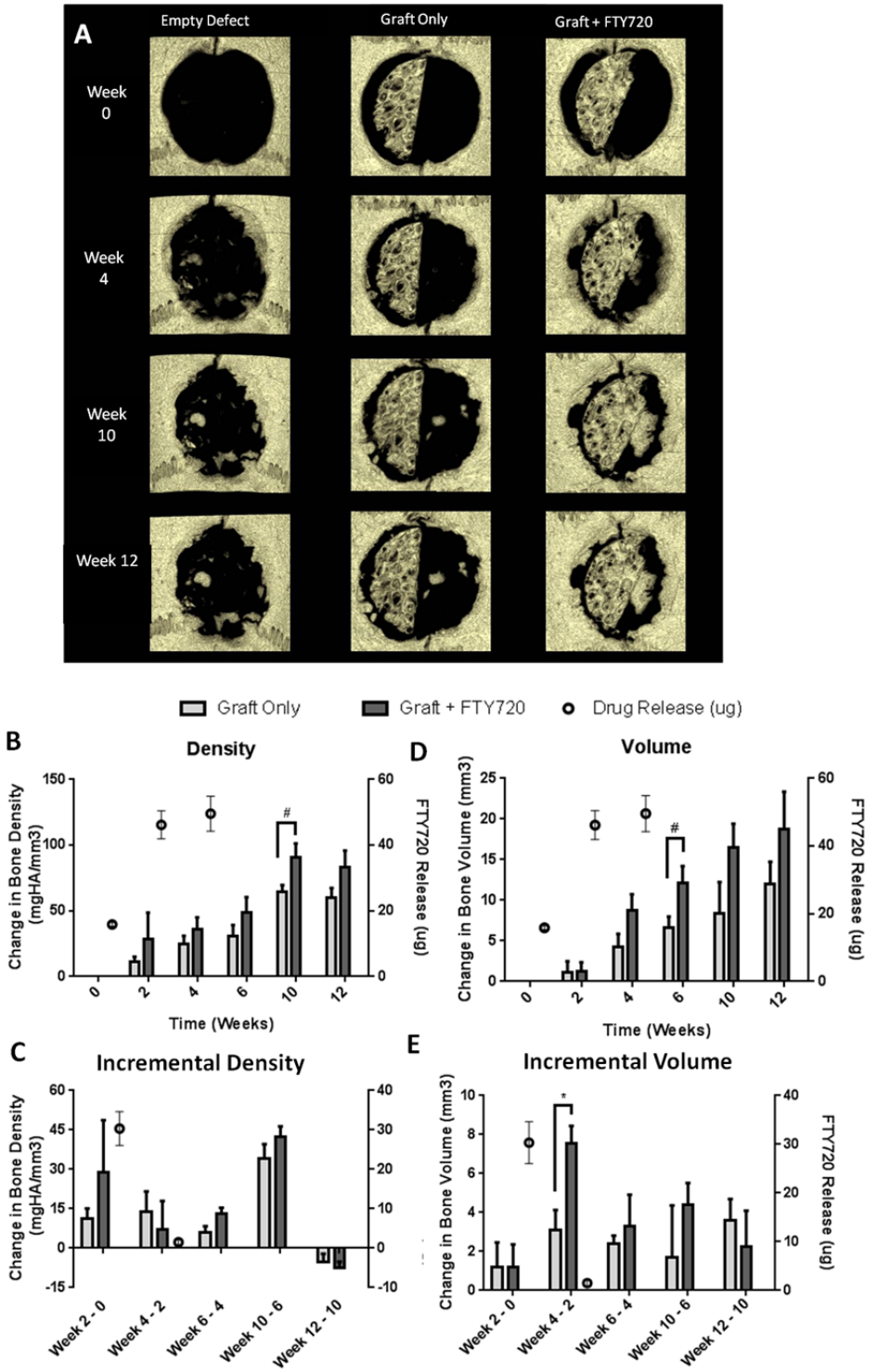

Fig 3.9: FTY720 increases bone regeneration in cranial defect. A) uCT reconstructions of rat cranial defects implanted with FTY720-coated human trabecular allografts. uCT evaluation of B) cumulative bone density, C) incremental bone density, D) cumulative bone volume and E) incremental bone volume compared to FTY720 release.

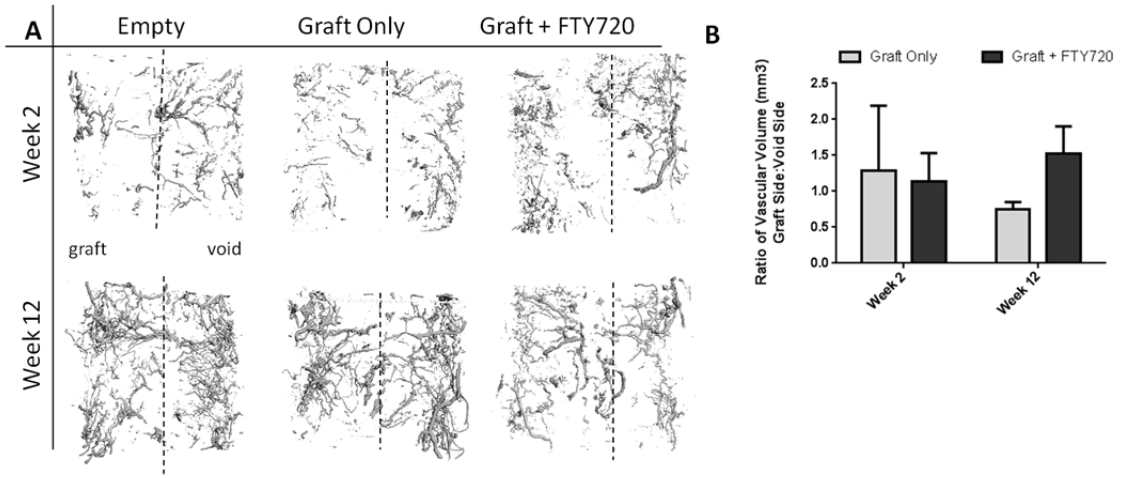

Fig 3.10: FTY720 improves vascularization on the graft side of the cranial defect. A) MICROFIL-assisted uCT imaging of vascularization in defect area. B) Ratio of vascularization on graft side: void side increases with FTY720.

3.4.3 FTY720 recruits progenitor cells to the defect area

Massons Trichrome and hematoxylin and eosin staining allow visualization of the tissue composition of the wound area. It is apparent that the addition of the graft improved bone deposition in both the graft and void side compared to the empty and graft only defects (Fig 3.11). By twelve weeks, the pores in the human trabecular graft in the FTY720 group have begun filling with new bone mineral, whereas in the graft only group the pores still appear empty. Immunohistochemical staining (Fig 3.12) was performed, and images were taken in three regions as indicated by the figure: firstly, in the bridge region between the graft and host bone, second in the middle of the graft region, and third, in the center of the void space. Staining revealed that FTY720 qualitatively increased the amount of CD90 and CD29 positive osteoprogenitor cells in the defect compared to the graft only group. Additionally, there is an increase in CD34+ endothelial cells in the drug treated group. Finally, we see a qualitative decrease in CD68+ macrophages in the drug treated group, suggesting possible immunosuppression with application of FTY720. All these observations are still qualitative, and require further staining and analysis.

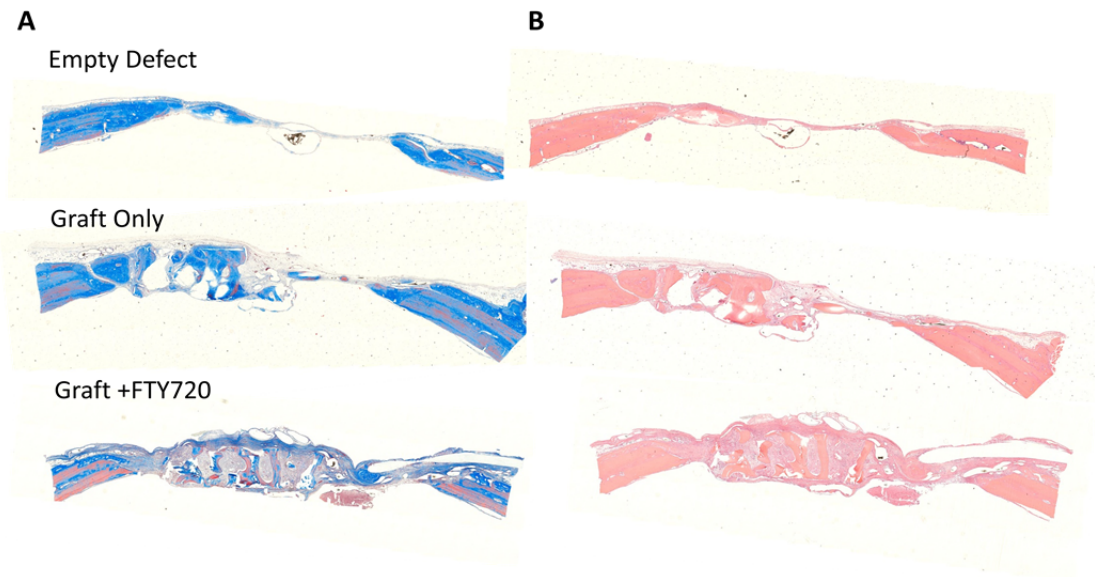

Fig 3.11: Histological staining of rat cranial defect at 12 weeks. A) Masson trichrome and B) H&E.

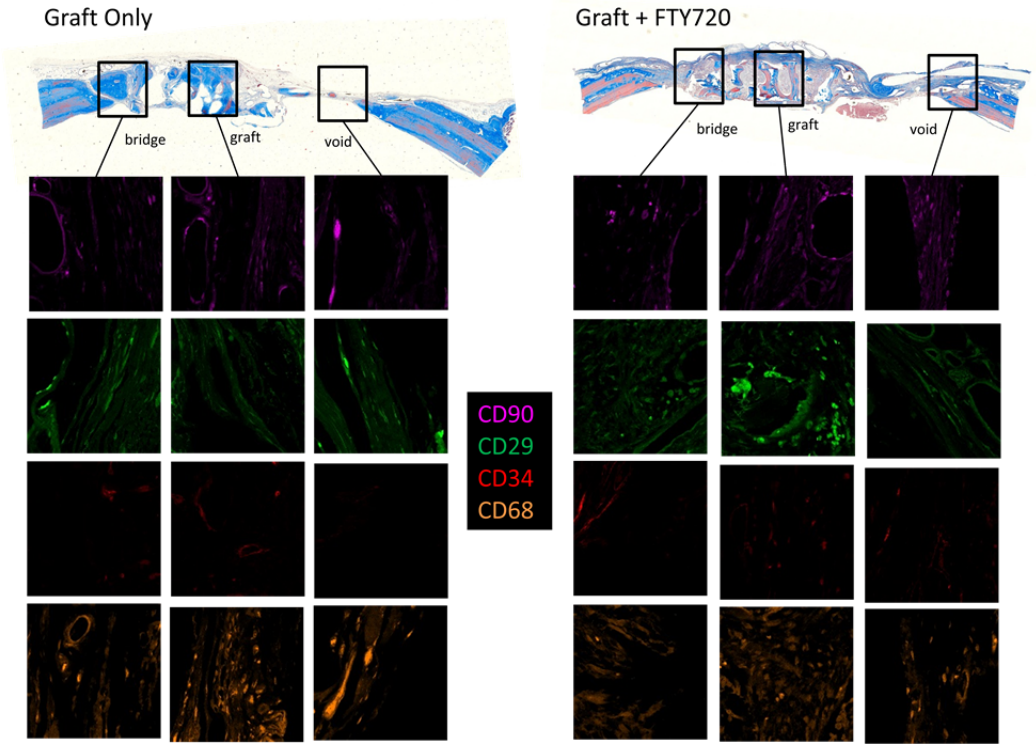

Fig 3.12: FTY720 increases recruitment of progenitor cells and reduces recruitment of macrophages in rat cranial defect.

CHAPTER 4

SUMMARY

There remains a clinical need for effective therapies for bone regeneration and graft integration for a variety of bone defects. Autografts remain the gold standard because of their low immunogenicity, as well as their high osteoconductivity and osteoinductivity. However, there still remains the complication that autograft bone material is scarce, and harvested autograft bone may not have the size or structural compatibility with the wound area.

The studies in this thesis present the use of FTY720 to improve the osteoconductivity and osteoinductivity of bone allografts. The release of FTY720 from PLAGA-coated bone allografts in rat cranial defects, from PLAGA-grafts in rat tibial defects, from Matrigel plugs in mouse tibial defects, and from direct adsorption onto human bone xenografts in rat cranial defects is shown to improve bone regeneration in the defect area. Additionally, vascularization into the graft is increased, indicating improve graft integration compared to treatments containing no FTY720. Finally, it is demonstrated that FTY720 creates a local immunosuppressive environment when a decellularized human graft is implanted into a rat defect model.

For future consideration of applying FTY720 for bone regeneration in a clinical setting, an effort was made to remove the PLAGA component from the drug-loading strategy onto grafts. A survey of literature and current available treatments show that despite the large number of PLAGA-based technologies used in animal studies for bone regeneration and other therapies, a much smaller number of those technologies reach clinical trials. Therefore, we evaluated a drug-loading strategy onto bone grafts that did

not require a PLAGA component to facilitate binding of FTY720 to the graft surface and saw that it performed as well as a similar graft that did contain PLAGA.

In conclusion, the results in this thesis show that FTY720 is efficacious in improving bone regeneration and vascularization in bone defects, reduces immunogenicity of foreign grafts, and that FTY720 can be loaded onto bone grafts without the use of a polymer phase. As we begin to more thoroughly characterize the origins of the cells that are recruited to the wound area by FTY720, improved immunohistochemical, and possibly flow based methods will need to be developed and verified to more accurately characterize the cell composition in the wound space.

REFERENCES

[1] Jacobs JJ, Anderson GB, Bell JE, Weinstein SL, Dormans JP, Gnatz SM, Lane N, Puzas JE, St. Clair EW, and Yelin EH. "The burden of musculoskeletal disease in the United States," American Academy of Orthopaedic Surgeons, 2008.

[2] HCUP Agency for Healthcare Research and Quality. "2011 National Statistics – Principal Procedure", http://hcupnet.ahrq.gov/HCUPnet.jsp (Accessed Nov 1, 2013).

[3] Jahangir AA, Nunley RM, Mehta S, Sharon A, and the Washing Health Policy Fellows. "Bone graft substitutes in orthoepaedic surgery," American Academy of Orthopaedic Surgeons Now, 2008.

[4] Burchardt H. "The biology of bone graft repair," *Clincal Orthopaedics and Related Research,* 1983, 174: 28-42.

[5] Bauer TW, and Muschler GF. "Bone graft materials," *Clinical Orthopaedics and Related Research,* 2000, 371:10-27.

[6] Lee SH, and Shin H. "Matrices and scaffolds for delivery of bioactive molucules in bone and cartilage tissue engineering," *Advanced Drug Delivery Reviews,* 2007, 59: 339-359.

[7] Cook SD, Wolfe MW, Sakeld SL, and Rueger DC. "Effect of recombinant human osteogenic protein-1 on healing of segmental defects in non-human primates," *The Journal of Bone and Joint Surgery,* 1995, 77(5): 734-750.

[8] Jefferies SR, inventor. July 19,1983. "Bone graft material for osseos defects and method of making same," United States Patent 4394370.

[9] Laurencin C, Khan Y and El-Amin SF. "Bone graft substitutes," *Expert Reviews of Medical Devices,* 2006, 3(1): 49-57.

[10] Burdick JS, and Anseth KS. "Photoencapsulation of osteoblasts in injectable RGD-modified PEG hydrogels for bone tissue engineering," *Biomaterials,* 2002, 23: 4315-4323.

[11] Saito N, Okada T, Horiuchi H, Murakami N, Takahashi J, Nawata M, Ota H, Nozaki K, and Takaoka K. "A biodegradable polymer as a cytokine delivery system for inducing bone formation," *Nature Biotechnology,* 2001, 19: 332-335.

[12] Ahlmann E, Patzakis M, Roidis N, Shepherd L, and Holtom P. “Comparison of anterior and posterior iliac crest bone grafts in terms of harvest-site morbidity and functional outcomes,” *Journal of Bone and Joint Surgery*, 2002, 84A(5), 716-720.

[13] Summers BN, and Eisenstein SM. “Donor site pain from the ilium,” *Journal of Bone and Joint Surgery*, 1989, 71B(4): 677-680.

[14] Giannoudis PV, Dinopoulos H, and Tsiridis E. “Bone substitutes: An update,” *Injury*,2005, 365:S20-S27.

[15] Dimitriou R, Mataliotakis GI, Angoules AG, Kanakaris NK, and Giannoudis PV. “Complications following autologous bone graft harvesting from the iliac crest using the RIA: A systematic review,” *Injury*, 2011, 42:S3-S15.

[16] Brydone AS, Meek D and Maclaine S. “Bone grafting, orthopaedic biomaterials, and the clinical need for bone engineering,” *Proceedings of the Institution of Mechanical Engineerings: Journal of Engineering in Medicine*, 2010, 224H: 1329-1343.

[17] Jackson DW, Windler GE, and Simon TM. “Intraarticular reaction associated with the use of freeze-dried, ethylene oxide-sterilized bone-patella tendon-bone allografts in the reconstruction of the anterior cruciate ligament,” *Americal Journal of Sports Medicine*, 1990, 18(1): 1-11.

[18] Pelker RR, Friedlaender GE, and Markham TC. “Biomechanical properties of bone allografts,” *Clinical Orthopaedics and Related Research*, 1983, 174: 54-57.

[19] Kaku N, Tsumura H, Kataoka M, Taira H, and Torisu T. “Influence of aeration, storage, and rinsing condtions on residual ethylene oxide in freeze-dried bone allograft,” *Journal of Orthopaedic Science*, 2002, 7: 238-242.

[20] Delloye C, Cornu , Druez V, and Barbier O. “Bone Allografts: What they can offer and what they cannot,” *Journal of Bone and Joint Surgery*, 2007, 89B(5): 574-580.

[21] Wheeler DL, and Enneking WF. “Allograft bone decreases in strength in vivo over time,” *Clinical Orthopaedics and Related Research*, 2005, 435: 36-42.

[22] Zhang X, Xie C, Lin ASP, Ito H, Awad H, Lieberman JR, Rubery PT, Schwarz ED, O’Keefe RJ, and Guldberg RE. “Periosteal progenitor cell fate in segmental cortical bone graft transplantations Implications for functional tissue engineering,” *Journal of Bone and Mineral Research*, 2005, 20(12): 2124-2137.

[23] Ishii M, Egen JG, Klauschen R, Meier-Schellersheim M, Saeki Y, Vacher J, Proia RL, and Germain RN. “Sphingosine-1-phosphate mobilizes osteoclast precursors and regulates bone homeostasis,” *Nature*, 2009, 458(7237): 524-528.

[24] Ryu J, Kim HJ, Chang E, Huang H, Banno Y, and Kim H. “Sphingosine 1-phosphate as a regulator of osteoclast differentiation and osteoclast-osteoblast coupling,” *The EMBO Journal*, 2006, 25(24): 5840-5851.

[25] Pederson L, Ruan M, Westendorf JJ, Khosla S and Oursler MJ. “Regulation of bone formation by osteoclasts involves Wnt/BMP signaling and the chemokine sphingosine-1-phosphate,” *Proceedings of the National Academy of Science*, 2008, 105(52): 20764-20769.

[26] Golan K, Vagima Y, Ludin A, Itkin T, Cohen-Gur S, Kalinkovich A, Kollet O, Kim C, Schajnovitz A, Ovadya Y, Lapid K, Shivtiel S, Morris AJ, Patajczak MA, and Lapidot T. “S1P promotes murine progenitor cell egress and mobilization via $S1P_1$-mediated ROS signaling and SDF-1 release,” *Blood*, 2012, 119: 2478-488.

[27] Takuwa Y, Du W, Qi X, Okamoto Y, Takuwa N, and Yoshioka K. “Roles of sphingosine-1-phosphate signaling in angiogenesis,” *World Journal of Biological Chemistry*, 2010, 1(10): 298-306.

[28] Lee M, Thangada S, Claffey KP, Ancellin N, Liu CH, Kluk M, Volpl M, Sha’afl RI, and Hla T. “Vascular endothelial cell adherens junction assempby and morphogenesis induced by Sphingosine-1-Phosphate,” *Cell*, 1999, 99: 301-312.

[29] Lee M, Thangada S, Paik J, Sapkota GP, Ancellin N, Chae S, Wu M, Morales-Ruiz M, Sessa WC, Alessi D and Hla T. “Akt-mediated phosphorylation of the G protein-coupled receptor EDG-1 is required for endothelial cell chemotaxis,” *Molecular Cell*, 2001, 8: 693-704.

[30] Allende ML, Yamashita T, and Proia RL. “G-protein-coupled receptor $S1P_1$ acts within endothelial cells to regulate vascular maturation,” *Blood*, 2003, 102: 3665-3667.

[31] Olivera A, and Spiegel S. “Sphingosine-1-phosphate as second messenger in cell proliferation induced by PDGF and FCS mitogens,” *Nature*, 1993, 35: 557-560.

[32] Guo X, Zheng Q, Kulbatski I, Yuan Q, Yang S, Shao Z, Wang H, Xiao B, Pan Z, and Tang S. “Bone regeneration with active angiogenesis by basic fibroblast growth factor gene transfected mesenchymal stem cells seeded on porous β-TCP ceramic scaffolds,” *Biomedical Materials*, 2006, 1:93-99.

[33] Schwab SR, Pereira JP, Matioubian M, Xu Y, Huang Y, and Cyster JG. “Lymphocyte sequestration through S1P lyase inhibition and disruption of S1P gradients,” *Science*, 2005, 309: 1735-1739.

[34] Hughes JE Srinivasan S, Lynch KR, Proia RL, Ferdek P, Hedrick CC. “Spingosine-1-phosphate induces an anti inflammatory phenotype in macrophages,” *Circulation Research*, 2008, 102(8): 950-958.

[35] Awojoodu AO, Ogle ME, Sefcik LS, Bowers DT, Martin K, Brayman KL, Lynch KR, Peirce-Cottler SM, Botchwey E. “Sphingosine 1-phosphat receptor 3 regulates recruitment of anti-inflammatory monocytes to microvessels during implant arteriogenesis,” *Proceedings of the National Academy of Science,* 2013, 110(34): 13785-13790.

[36] Sharma S, Mathur AG, Pradhan S, Singh DB, and Gupta S. “Fingolimod (FTY720): First approved oral therapy for multiple sclerosis,” *Journal of Pharmacology and Pharmacotherapeutics,* 2011, 2(1): 49-51.

[37] Kovarik JM, Schmouder R, Barilla D, Wang Y and Kraus G. “Single dose FTY720 pharmacokinetics, food effect, and pharmacological responses in healthy subjects,” *British Journal of Clinical Pharmacology,* 2004, 57(5): 586-591.

[38] Petrie Aronin CE, Sefcik LS, Tholpady SS, Tholpady A, Sadik KW, Macdonald TL, Peirce-Cottler SM, Wamhoff BR, Lynch KR, Ogle RC, and Botchwey EA. “FTY720 promotes local microvascular network formation and regeneration of cranial bone defects,” *Tissue Engineering Part A,* 2010, 16(6): 1801-1809.

[39] Petrie Aronin CE, Shin SJ, Naden KB, Rios PD, Sefcik LS, Zawodny SR, Bagayoko ND, Cui Q, Khan Y, and Botchwey EA. “The enhancement of bone allograft incorporation by the local delivery of the sphingosine 1-phosphate receptor targeted drug FTY720,” *Biomaterials,* 2010, 31(25): 6417-6424.

[40] Das A, Tanner S, Barker DA, Green D, and Botchwey EA. “Delivery of S1P receptor-targeted drugs via biodegradable polymer scaffolds enhances bone regeneration in a critical size cranial defect,” *Journal of Biomedical Materials Research Part A,* 2013, [article in press].

[41] Das A, Segar CS, Hughley BB, Bowers DT, and Botchwey EA. “The promotion of mandibular defect healing by the targeting of S1P receptors and the recruitment of alternatively activated macrophages,” *Biomaterials,* 2013, [article in press].

[42] Sato C, Iwasaki T, Kitano S, Tsunemi S, and Sano H. “Sphingosine 1-phosphate receptor activation enhances BMP-2 induced osteoblast differentiation,” *Biochemical and Biophysical Research Communications,* 2012, 423: 200-205.

[43] Sefcik LS, Petrie Aronin CE, Awojoodu AO, Shin SJ, Mac Gabhann F, Macdonald TL, Wamhoff BR, Lynch KR, Peirce-Cottler SM, and Botchwey EA. “Selective activation of sphingosine 1-phosphate receptors 1 and 3 promotes local microvascular network growth,” *Tissue Engineering Part A,* 2011, 17(5-6): 617-629.

[44] Mandela S, Hajdy R, Bergstrom J, Quackenbush E, Xie J, Milligan J, Thornton R, Shei G, Card D, Keohane C, Rosenbach M, Hale J, Lynch CL, Rupprecht K, Parsons W, and Rosen H. “Alteration of lymphocyte trafficking by sphingosine-1-phosphate receptor agonists,” *Science,* 2002, 296(346): 346-349.

[45] Brinkmann V, Davis MD, Heise CE, Albert R, Cottens S, Hof R, Bruns C, Prieschl E, Baumruker T, Hiestand P, Foster CA, Zollinger M, and Lynch KR. The immune modulator FTY720 targets sphingosine 1-phosphate receptors," *Journal of Biological Chemistry,* 2002, 277: 21463-21467.

[46] Ying Y, Wang L, Chen Y, Jiang J, Ouyang Y, Huang H, and Xu J. "FTY720 and cyclosporin protect ovarian tissue grafted into rabbits," *European Journal of Obstetrics & Gynecology and Reproductive Biology,* 2013, [article in press].

[47] Semete, B, Booysen L, Lemmer Y, Kalombo L, Katata L, Verschoor J, and Swai H. "In vivo evaluation of the biodistribution and safety of PLGA nanoparticles as drug delivery systems," *Nanomedicine,* 2010, 6: 662-671.

[48] Anderson JM, and Shive MS. "Biodegradation and biocompatibility of PLA and PLGA microspheres," *Advanced Drug Delivery Reviews, 5-24.*

[49] Ji W, Yang F, Seyenejad H, Chen Z, Hennink WE, Anderson JM, can den Buecken JJJP, and Jansen JA. "Biocompatibility and degradation characteristics of PLGA-based electrospun nanofibrous scaffolds with nanoapatite incorporation," *Biomaterials,* 2012, 33: 6604-6614.

[50] Lu J, Wang X, Marin-Muller C, Wang H, Lin PH, Yao Q, and Chen C. "Current advances in research and clinical applications of PLGA-based nanotechnology," *Expert Review of Molecular Diagnostics,* 2009, 9(4): 325-341.

[51] Yoshimoto H, Shin YM, Terai H, and Vacanti JP. "A biodegradable nanofiber scaffold for electrospinning and its potential for bone tissue engineering," *Biomaterials,* 2003, 24: 2077-2082.

[52] Panyam J, Zhou W, Prabha S, Sahoo SK, and Labhasetwar V. "Rapid endo-lysosomal escape of poly(DL-lactide-co-glycolide) nanoparticles: implications for drug and gene delivery," *The FASEB Journal,* 2002, 16: 1217-1226.

[53] Klose D, Siepmann F, Elkharraz K, and Siepmann J. "PLGA-based drug delivery systems: Importance of the type of drug and device geometry," *International Journal of Pharmaceutics,* 2008, 354: 95-103.

[54] Bala J, Hariharan S, Kumar MN. "PLGA nanoparticles in drug delivery: the state of the art," *Critical Reviews of Therapeutic Drug Carrier Systems,* 2004, 21(5): 387-422.

[55] Kaigler D, Wang Z, Horger K, Mooney DJ, and Krebsbach PH. "VEGF scaffolds enhance angiogenesis and bone regeneration in irradiated osseous defects," *Journal of Bone and Mineral Research,* 2006, 21(5): 735-744.

[56] Kent Leach J, Kaigler D, Wang Z, Krebsbach PH, and Mooney DJ. “Coating of VEGF-releasing scaffolds with bioactive glass for angiogenesis and bone regeneration,” *Biomaterials,* 2006, 27: 3249-3255.

[57] de Guzman RC, Saul JM, Ellenburg MD, Merrill MR, Coan HB, Smith TL and Van Dyke ME. “Bone regeneration with BMP-2 delivered from keratose scaffolds,” *Biomaterials,* 2013, 34: 1644-1656.

[58] Lee SS, Huang BJ, Kaltz SR, Sur S, Newcomb CJ, Stock SR, Shah RN, and Stupp SI. “Bone regeneration with low dose BMP-2 amplified by biomimetic supramolecular nanofibers within collagen scaffolds,” *Biomaterials,* 2013, 34: 452-459.

[59] Zara JN, Siu RK, Zhang X, Shen J, Ngo R, Lee M, Li W, Chiang M, Chung J, Kwak J, Wu BM, Ting K, and Soo C. “High doses of bone morphogenetic protein 2 induce structurally abnormal bone and inflammation in vivo,” *Tissue Engineering Part A.* 2011, 17(9-10): 1389-199.

[60] Huang C, Das A, Barker D, Tholpady S, Wang T, Cui Q, Ogle R, and Botchwey EA. “Local delivery of FTY720 accelerates cranial allograft incorporation and bone formation,” *Cell and Tissue Research,* 2012, 347(3): 553-566.

[61] Kansas Joint and Spine Institute. “Outcomes of degenerative disc disease patients treated with an anterior-only fusion using InQu bone graft”, In: ClinicalTrials.gov [Internet]. Bethesda (MD): National Library of Medicine (US). 2000-[2013 Oct 15]. Available from: http://clinicaltrialsfeeds.org/clinical-trials/show/NCT01746212. NLM Identifier: NCT01746212.

[62] ISTO Technologies. “InQu as a Bone Graft Substitute”, www.isotech.com/inqu-orthopedics.html (Accessed Oct 10, 2013).

[63] Stewart, G. “Sustainable bone volume in a single level posterolateral lumbar arthrodesis receiving InQu bone graft extender,” http://www.istotech.com/case-report-stewart.html (Accessed Nov 5, 2013).

[64] Niemalä S, Ikäheimo I, Koskela M, Veiranto M, Suokas E, Törmälä P, Waris T, Ashammakhi N, Syrjälä H. “Ciprofloxacin-releasing bioabsorbable polymer is superior to titanium in preventing *Staphylococcus epidermis* attachment and biofilm formation in vitro,” *Journal of Biomedical Materials Research Part B,* 2005, 76B(1): 8-14.

[65] Boston Scientific Corporation. “The EVOLVE II clinical trial to assess the SUNERGY stent system for the treatment of atherosclerotic lesion(s),” In: ClinicalTrials.gov [Internet]. Bethesda (MD): National Library of Medicine (US). 2000-[2013 Sept 17]. Available from: http://clinicaltrialsfeeds.org/clinical-trials/show/NCT01665053. NLM Identifier: NCT01665053.

[66] Muramatsu T, Onuma Y, Zhang Y, Bourantas CV, Kharlamov A, Diletti R, Farooq V, Gogas BD, Garg S, Garcia-Garcia HM, Ozaki Y, and Serruys PW. "Progress in treatment by percutaneous coronary intervention: The stent of the future," *Revista Española de Cardiologia,* 2013, 66(6): 483-496.

[67] Meredith IT, Verheye S, Dubois CL, Dens J, Fajadet J, Carrié, Walsh S, Oldroyd KG, Varenne O, El-Jack S, Moreno R, Joshi AA, Allocco DJ, and Dawkins KD. "Primary endpoint results of the EVOLVE trial," *journal of the American College of Cardiology,* 2012, 59: 1362-1370.

[68] Olivier JC, Fenart L, Chavet R, Pariet C, Cecchilli R, Couet W. "Indirect evidence that drug brain targeting using polysorbate 80-coated polybutlcyanoacrylate nanoparticles in related to toxicity," *Pharm Research,* 1999, 16: 1836-1842.

[69] Astaneh R, Erfan M, Moghimi H, and Mobedi H. "Changes in morphology of in situ forming PLGA implant prepared by different polymer molecular weight and its effect on release," *Pharmaceutics, Preformulation and Drug Delivery,* 2009, 98(1): 135-145.

[70] Reed AM, and Gilding DK. "Biodegradable polymers for use in surgery – poly(glycolic)/poly(lactic acid) homo and copolymers: 2. In vitro degradation," *Polymer*, 1981, 22: 494-498.

[71] Viguet-Carrin S, Garnero P, and Delmas PD. "The role of collagen in bone strength," *Osteoporosis International,* 2006, 17: 319-336.

[72] Wu N, Lee Y, Segina D, Murray H, Wilcox T, Boulanger L. "Economic burden illness among US patients experiencing fracture nonunion," *Orthopedic Research and Reviews*, 2013, 5: 21-33.

[73] Bax BE, Wozney JM, and Ashhurst DE. "Bone morphogenetic protein-2 increases the rate of callus formation after fracture of the rabbit tibia," *Calcified Tissue International,* 1999, 63: 83-89.

[74] McKibbin B. "The biology of fracture healing in long bones," *Journal of Bone and Joint Surgery*, 1978, 60B: 150-162.

[75] Yu H, VandeVord PJ, Matthew HW, Wooley PH, and Yang S. "Improved tissue-engineered bone regeneration by endothelial cell mediated vascularization," *Biomaterials,* 2009, 30: 508-517.

[76] Jones AL, Bucholz RW, Bosse MJ, Mirza SK, Lyon TR, Webb LX, Pollak AN, Golden JD, and Valentin-Opran A. "Recombinant human BMP-2 and allograft compared with autogenous bone graft for construction of diaphyseal tibial fractures with cortical defects," *Journal of Bone and Joint Surgery,* 2006, 88A(7): 1430-1441.

[77] Sefcik LS, Petrie Aronin CE, Wieghaus KA, and Botchwey EA. “Sustained release of sphingosine 1-phosphate for therapeutic arteriogenesis and bone tissue engineering,” *Biomaterials,* 2008, 29(19): 2869-2877.